The Mechanical Behavior of Chalk under Laboratory Conditions Simulating Reservoir Operations

by

Edvard Omdal

Thesis submitted in fulfillment of
the requirements for the degree of
PHILOSOPHIAE DOCTOR
(PhD)

University of
Stavanger

FACULTY OF SCIENCE AND TECHNOLOGY
DEPARTMENT OF PETROLEUM ENGINEERING
2010

University of Stavanger
N-4036 Stavanger
NORWAY
www.uis.no

ISBN: 978-82-7644-414-8
ISSN: 1890-1387

Summary

This work has been carried out with the chalk mechanics research society at the University of Stavanger. The PhD thesis is thus a continuation to the long line of experimental chalk research carried out honoring the academic principles investigating fundamental mechanisms of chalk mechanical behavior. Simultaneously, the work and objectives have been a joint project with the Ekofisk license (the COREC program) and the Valhall license ensuring a strong link to important operating challenges associated with hydrocarbon production from chalk reservoirs. The overall goal has been to address fundamental chalk behavior in a controlled laboratory environment and simultaneously approach conditions as close as possible as those in-situ. The focus in this thesis may be subdivided into five main categories:

- Experimental challenges regarding the effective stress relations.
- Time and rate effects during depletion close to in-situ conditions.
- Seawater impact on creep close to in-situ conditions.
- Basic mechanisms for chemical water weakening.
- Effect of acid injection as a function of various chalk properties.

The contribution of the pore fluid pressure to the reduction of the effective stress during loading of fully saturated high porosity chalk (>40% porosity) has often been assumed to be represented by an effective stress coefficient close to unity. **Paper I** presents laboratory experiments that were conducted by simultaneously increasing total stress and pore pressure. These tests resulted in substantial strains that should not occur if the assumption of an effective stress coefficient close to unity was true. The significant strains detected therefore led to the initiation of a subsequent study focusing on the effective stress coefficient for porous chalk material. The results from **paper I** suggest that the effective stress coefficient for high porosity outcrop chalks depends on the applied stress and the pore fluid, and is thus not a constant, nor close to unity as commonly presumed. The findings from **paper I** led to a re-evaluation of chalk strength, as hydrostatic yield was measured at various levels of pore pressure in **paper II**. These results indicate agreement with the theoretical assumptions stating that the effective stress coefficient is close to unity for high porosity chalk. The contradiction between **paper I** and **paper II** is interpreted as effects of inelasticity, which have impact on the compressibility while the strength seems unaffected.

A laboratory test program, which simulated reservoir depletion was conducted on outcrop and reservoir chalk samples of various porosities (**paper III**). All the samples experienced a uniaxial stress path that led to compaction failure, i.e. pore collapse. This depletion phase was followed by a creep period, where time-dependent deformation was monitored. The results of **paper III** show that chalk is indeed a rate-dependent material under laboratory loading conditions as time effects were revealed

as the loading rate was varied. However, the results raise uncertainty about the importance of this rate dependency for chalk under completely drained conditions. Further, such high-porosity chalks suffer substantial plastic strains and significant strain hardening. Indeed, a relation between deformation/porosity and hardening is proposed by the introduction of real-time moduli values. **Paper III** also showed that transient creep is dependent on the stress history. The stress history also affects the uniaxial strain stress path. Both these effects of the stress history are related to the nucleus of failure concept. Ultimately, such time dependence on the stress path may contribute to the understanding of stress path data deduced from field data. **Paper IV** deals with the impact of load rate, pore collapse and fluid flow restrictions. **Paper IV** relates the artificial imposed flow restriction in the experiments to field scale effects like low permeability areas and the limited number of wells in a reservoir. Flow restrictions could cause partially drained conditions that may result in pore pressure increments at various locations within the reservoir. Knowing that reservoir porosity, which largely governs the yield strength of chalk, varies significantly in the North Sea chalk reservoirs, it could be interesting to take such effects into account.

The effects of the aqueous chemistry on the mechanical strength of chalk are studied in **paper V**. At high temperatures (~130 °C), chalk exposed to seawater is significantly weaker compared to chalk exposed to distilled water. In **Paper V** results from series of mechanical tests are presented and it was found that cores with small variations in mineralogy exhibit an unexpected difference in their mechanical response when comparing cores flooded with NaCl and $MgCl_2$ at 130 °C. Further, the results show that the weakening by magnesium seems to also be governed by a certain time dependency. Independent of the chalk type tested, the chemical analyses performed show that when $MgCl_2$ is flooded through the core, a significant loss of magnesium and a considerable additional amount of calcium is detected in the effluent. The experimental observations fit very well with the time dependent chemical changes gained from the mathematical model presented that accounts for transport effects and chemical processes. The calculations indicate that when magnesium is precipitated and forming new mineral phases, not only calcite, but also silicates are dissolved. Both the retention of magnesium in the chalk core and the formation of newly precipitated magnesium-bearing carbonates and/or magnesium-bearing clay-like minerals after flooding with $MgCl_2$ brine were demonstrated by scanning electron microscopic (SEM) studies. In addition, precipitation of anhydrite as a result of flooding with seawater-like brine was detected by SEM-images.

In **Paper VI** the water weakening of chalks is further investigated with the purpose of approaching more realistic reservoir conditions in laboratory experiments. Seawater is injected for pressure support in several North Sea chalk reservoirs, however, it has been shown that such injection significantly weakens the chalk. The subsidence of the seafloor is therefore not inhibited, rather promoted in some cases. The focus in **paper VI** has been the effect of synthetic seawater injection as a function of injected volume on chalk deformation. The main contribution from this study is the realistic experimental programme, combining low residual initial brine saturation, high (in-situ) testing temperature as well as high (in-situ) pore pressure, which all add significantly to the complexity of the experimental procedure. **Paper VI** shows that

cores flooded with synthetic seawater close to reservoir condition obtain increased water induced compaction and the magnitude seems to depend on the injected volume. The axial creep rate seems to be permanently changed after relatively limited volume of water injected. The dependence on volume injected indicates that the water weakening effect is related to ongoing chemical reactions as presented in **Paper V** which may be described by thermodynamically aqueous equilibrium chemistry.

Finally, in **paper VII** the effect of hydrochloric acid injection in chalk cores is studied. The chalk formations are characterized by high $CaCO_3$ content which makes the rock highly soluble in acids. Accordingly, acid stimulation is frequently used to increase well injectivity or productivity. Previous investigations suggest the acid to create wormholes, however, casing deformations and production-log results combined with the stimulation rates and pressures used, indicate that other geometries may develop. The objective has been to test existing theories by stimulating chalk using different core setups in a tri-axial cell. The experimental results presented in **Paper VII** confirm the importance of rock properties and flooding regime for the acid etched geometry. It is suggested that the acid is most likely forming a cavity around the liner for the typical field stimulation rates and pressures used in North Sea chalks.

The significance of this work may be summarized in five main findings:

- The experimentally determined effective stress coefficient, α, differs significantly from the theoretical predicted, when compressibility is used as basis for the evaluation.

- The experimental results show that high porosity chalk cores with similar porosity, depleted with considerably different load rates obtain similar amount of final deformation. This raise uncertainty about the importance of rate dependency of chalk under completely drained conditions.

- A load rate dependency on the uniaxial strain stress path has been demonstrated. Further, the development of transient creep show similar dependency considering load rate. The PhD thesis relates both these findings to the evolution for failure at grain scale, as described by the nucleus of failure concept.

- Seawater injection at elevated temperatures chemically weakens the chalk. The degree of weakening is primarily seen by the demonstrated volume effect; a core subjected to continuous injection of synthetic seawater weakens significantly more than cores subjected to limited volume injection. Evidence of newly precipitated minerals as a result of core flooding confirms ongoing dissolution-precipitation processes taking place.

- The acid stimulation study suggests, through visual inspection of acidized cores, that porosity, permeability and material strength influence the created geometry. The acid seems to spread more easily in higher porosity and softer chalk.

Acknowledgements

Firstly, I acknowledge Merete V Madland who has been the academic responsible and main supervisor of this thesis. She became my supervisor during my undergraduate work back in 2004, and her encouragement and support has followed me since. Thanks for giving my academic interest direction which empowered me to do this thesis. Her sense for details have kept me focused and helped me communicating the content of this work.

I would also like to thank my supervisors Tron G Kristiansen, Reidar I Korsnes and Aksel Hiorth. Trons experience and overview on the subject and geomechanics in general has helped put my topic in perspective. Reidar is remembered for his enthusiasm and dedication to chalk research. A special thank goes to my industry mentor Neal B Nagel for organizing my internship at the Rock and Fracture Mechanics Laboratories at the Bartlesville Technology Center of ConocoPhillips in Oklahoma.

The ambitious experimental program of this thesis would not have been possible without the help of Svein Myhren and Kim Andre N Vorland. Thanks also to David Chancellor and Rico Ramos and the rock mechanics community in Bartlesville for both technical support and hospitality. Thanks also to my colleagues and fellow students, especially Bizhan Zangiabadi and Megawati. Experimental work is often associated with frustration, and it has been nice to share this with good friends in the office and the lab. Tania Hildebrand-Habel, Unni Hakli, Skule Strand and Kjetil Ormark are all acknowledged for their good help. Thanks to all the students that I have worked with during the many hours in the lab, often after regular hours and sometimes overnight monitoring every reading.

I owe me deepest gratitude to my family and my wife in particular. She has paid the price of having a husband occupied with chalk research too many hours during the past years. Thanks for your patience and support.

ConocoPhillips Skandinavia AS and the Ekofisk covertures, (Total E&P Norge AS, Eni Norge AS, Statoil Petroleum AS and Petoro AS) through the research program COREC, and also BP Norge AS and the Valhall co-venturers (Hess Norge AS, A/S Norske Shell, and Total E&P Norge AS) are acknowledged for financial support. Thanks also to my current supervisor Ole Eeg for his recognitions of this work.

List of papers

I. **Omdal E, Breivik H, Næss KE, Kristiansen TG, Korsnes RI, Hiorth A, Madland MV (2009)** Experimental Investigation of the Effective Stress Coefficient for various High Porosity Outcrop Chalks.

   a. *First presented at the SCA conference, Abu Dhabi (2008)*

   b. *Proceedings of the 43rd US Rock Mechanics Symposium and 4th US-Canada Rock Mechanics Symposium, Asheville, ARMA 09-118*

II. **Madland MV, Omdal E, Breivik H, Korsnes RI, Hiorth A, Kristiansen TG (2009)** Investigation of the Effective Stress Relation for Outcrop Chalk. In: Ling HI, Smyth A, Betti R (eds), Poromechanics IV, 4th Biot Conference on Poromechanics. New York, DEStech Publication: 429-434

III. **Omdal E, Madland MV, Kristiansen TG, Nagel NB, Korsnes RI, Hiorth A, (2010)** Deformation Behavior of Chalk studied close to In-Situ Reservoir Conditions, Rock Mech Rock Eng *DOI 10.1007/s00603-010-0087-4*

IV. **Omdal E, Madland MV, Renli R, Kristiansen TG, Hiorth A, Korsnes RI, Hildebrand-Habel T (2009)** Laboratory Observation with Implications for Depletion of Chalk Reservoirs. In: Ling HI, Smyth A, Betti R (eds), Poromechanics IV, 4th Biot Conference on Poromechanics, New York, DEStech Publication: 953-958

V. **Madland MV, Omdal E, Megawati M, Hildebrand-Habel T, Korsnes RI, Evje S, Cathles L, Hiorth A (*accepted with minor revisions*)** Chemical alternations induced by rock-fluid interactions when injecting brines in high porosity chalks, Transp Porous Med

VI. **Omdal E, Madland MV, Kristiansen TG, Korsnes, RI, Nagel NB, Hiorth A, (*under review*)** Creep and Water Weakening of Chalk at High Pore Pressure and Temperature. Rock Mech Rock Eng

VII. **Omdal E, Dirdal E, Ormark K, Vorland KAN, Korsnes RI, Kristiansen TG, Knutsen TL, Hildebrand-Habel T, Madland MV (2008)** Induced Geometry in Chalk during Hydrochloric Acid Stimulation. In: Shao J-F, Burlion N (eds), Thermo-Hydromechanical and Chemical Coupling in Geomaterials and Applications. Proceedings of the 3rd International Symposium GeoProc'2008, Wiley: 187-194

Contents

1 Introduction

1.1 Chalks in Petroleum Context

For more than 30 years, deformation behavior of chalk has received considerable attention from petroleum operators and research communities. Several oilfields produce hydrocarbons from chalk formations in the southern parts of the Norwegian North Sea. The two most known are the Ekofisk and Valhall Fields. Common for both of these fields is that the reservoirs experience porosity reduction due to compaction of the chalk formations associated with field production (Pattillo et al., 1998; Sylte et al., 1999). The awareness of the significant potential for compaction of those reservoirs was raised by the discovery of severe seafloor subsidence at the Ekofisk Field in 1984 (Wiborg and Jewhurst, 1986). Since then, a vast amount of research has been conducted in order to understand the deformation behavior of chalk, and, in particular, the phenomenon known as water weakening.

1.1.1 Geological Aspects

The Maastrichtian chalk of north-west Europe was deposited in moderately shallow waters covering a large area from Poland in the east stretching into the Cretaceous Atlantic in the west (Håkansson et al., 1974). The Ekofisk (van den Bark and Thomas, 1981) and Valhall (Munns, 1985) Fields are both located within the Central Graben in the southern part of the Norwegian North Sea in this area of Maastrichtian chalk. In fact, both these fields produce hydrocarbons from the Tor Formation which is of Maastrichtian age. Geology categorizes chalk as a sedimentary rock within the carbonate rock family with a typical calcite content of >90%. The Tor formation is particularly clean and normally contains less than 5% non-carbonate minerals (e.g. Ruddy et al., 1989; Andersen, 1995). Maastrichtian outcrop chalks contain typically from 0.5% (Stevns Klint chalk in Denmark) to 17% (Hallembaye chalk in Belgium) non-carbonate minerals (Håkansson et al., 1974).

The grains, which make up the matrix structure, originate from skeletons of algae organisms that lived in oceanic pelagic environments. These skeletons of biogenetic origin are composed of carbonate, yet special for chalks is the stable polymorph of $CaCO_3$ that gives chalk great chemical stability (Scholle, 1977). The microscope image in Fig. 1.1 shows the grain structure of Kansas

chalk (see section 3.1.1), and a mixed composition of more or less intact skeleton fragments are seen. This is characteristic for chalks. As the deposited skeletons, called coccospheres were buried, geological processes caused them to end up as mostly coccoliths rings and rosettes and independent calcite plates, which is what Fig. 1.1 displays.

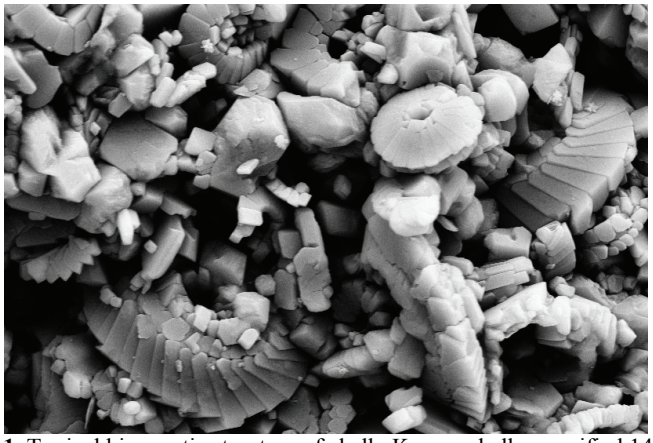

Fig. 1.1. Typical biogenetic structure of chalk, Kansas chalk magnified 14050X.

The chalk formations in the Central Graben of the North Sea are known for their remarkable storage capacity as a reservoir rock for the petroleum industry, and porosities up towards 50% are found at great depths (Munns, 1985). Such high porosity astonished geologists, as regular diagenesis would suggest a far lower porosity at the relevant depths. Scholle (1977) described this abnormal high porosity as a result of constraints on both physical and chemical compaction processes. Firstly, that the effect of overpressured reservoirs physically maintained the porosity as the overburden is supported by the fluid itself, and secondly, that early oil invasion and high oil saturation inhibited chemical induration of the chalk.

Despite this high porosity, the matrix permeability is relatively low. Sulak and Danielsen (1989) reported that the matrix permeability, even for high porosity chalk, is in the range of 1 - 5 mD. However, the effective permeability is much higher due to the natural fracture system in the reservoir, which enhances the permeability by a factor of 50 (Sulak and Danielsen, 1989).

1.1.2 Challenges for Chalk Reservoir Management

The operational history of the Ekofisk Field is reviewed only briefly to identify some of the challenges regarding oil recovery from chalk formations.

INTRODUCTION

Ekofisk became world famous during the tremendous elevation of platforms, the so-called Ekofisk Jacking Project, in the late 1980's (Smith et al., 1988). It was in November 1984 that the Phillips Petroleum Company identified the severe seabed subsidence. The reservoir management during early Ekofisk production involved pore pressure depletion, from initially 7000 psi (~48 MPa) towards 3500-4000 psi (~24-27 MPa) (Wiborg and Jewhurst, 1986). The high porosity chalk reservoir was experiencing significant porosity reduction due to this primary depletion, which resulted in reservoir compaction that propagated and caused subsidence of the seabed.

The depletion or primary production phase for Ekofisk was followed by a main water injection period that was initiated in 1988 (Gauer et al., 2002). This seawater injection, in addition to the Ekofisk Jacking Project, was expected to compensate for the subsidence problem. The pore pressure was still declining for some years after 1988, before it stabilized in 1994 and then slowly started to increase (Gauer et al., 2002). However, the authors report that the Ekofisk crestal 12-month subsidence rate remained high (0.4 m/year) until 1998, when it declined to 0.1 m/year. The seawater injection in Ekofisk was considered a success, as it contributed to a significant increase in oil production (Hermansen et al., 1997). However, the fact that the seabed is still compacting, even after pore pressure stabilization and increase, suggest that the chalk formation experiences substantial time dependent strains, and, as will be discussed in detail later, strains due to the water injection itself. Likewise, also the Valhall Field experiences similar management challenges and advantages as a high porosity and highly compressible chalk reservoir (Ruddy et al., 1989; York et al., 1992; Pattillo et al., 1998; Barkved et al., 2003; Kristiansen et al., 2005).

Due to the rather low matrix permeability and the high solubility of chalk in acid, acid is frequently used to treat formations by increasing the matrix permeability or by improving the conductivity of hydraulic fractures. Ekofisk has been stimulated, according to Snow and Brownlee, (1989), with pseudo limited entry, massive acid treatments, which for most cases creates acidized hydraulic fractures, yet matrix treatment also takes place in rare cases. Such pseudo limited entry design means that certain perforation intervals are selected for stimulation, contrary to injecting acid into the entire formation. Snow and Brownlee (1989) suggest that this design promotes fracture acidizing, which is the classical case in reservoir stimulation theory. The experience from acid fracturing at the Ekofisk Field shows that the increased productivity is rather short lived. Snow and Brownlee (1989) suggest that this is due to pore collapse and porosity reduction of high porosity chalk in the

reservoir in general, as well as the softness of chalk which causes the fractures to close.

1.2 Effective Stress Relations

Force distribution and how it is transfered in rocks is a complex physical scenario. Where forces in fluids act as a hydraulic pressure, forces transfer as stresses in solid materials. By using this definition, porous rocks may be described as a cross between fluids and solids. The pore space in porous sedimentary rocks contains fluids, while the solid part consists of the matrix of mineral grains. In a simple drained case, applied load is carried by the matrix structure alone, and the load is transferred at the many intergranular contacts. However, the pore fluid is very seldom perfectly drained, and most often obtain a certain hydraulic pressure. Which of these two competing factors, the hydraulic pore pressure or the external applied load, will have the greatest impact in the bulk volume of the porous rock specimen? Terzhagi (1923) proposed the concept of effective stress that describes this balance between the total stress (external applied load) and the pore pressure for a water saturated soil scenario. The effective stress σ', showed experimentally, was simply defined as the total stress σ minus the pore pressure P_P.

$$\sigma' = \sigma - \alpha \cdot P_P, \qquad (1.1)$$

The effective stress as shown in eq. 1.1 was further described (e.g. Skempton, 1961) by identifying a correction factor α for the pore fluid pressure, a so called poroelastic coefficient, Biot's factor or effective stress coefficient. The physical meaning of this coefficient is not very well defined or understood. The most accepted physical interpretation is probably the area ratio as described by Skempton (1961): Imagine two particles that share an intergranular contact. The area occupied by the intergranular contact over the total area of the grain defines the ratio of the grain surface not exposed to the pore pressure over the area of the grain. The coefficient, α, by this physical interpretation equals one minus this ratio. Such a physical understanding of the coefficient could be linked directly to cementation and packing of the grains. The most common engineering understanding of the coefficient relevant for the bulk volume change of porous material has been proposed according to eq. 1.2 (e.g. Fjær et al., 2008).

$$\alpha = 1 - \frac{C_s}{C_b} \qquad (1.2)$$

where C_s and C_b are the compressibility of the grains and bulk, respectively. Skempton (1961), however, claimed that this interpretation (eq. 1.2) not true for saturated rocks.

The effective stress concept was further described by Berryman (1992) who pointed out the importance of inhomogeneity of the rock matrix and discussed the existence of an independent effective stress coefficient for every rock property influenced by the pore pressure. In general, this means that the effect of pore pressure on the compressional wave velocity (e.g. Todd and Simmons, 1972) or shear wave velocity (e.g. Christensen and Wang, 1985) may be different than that of electrical conductivity of the bulk (e.g. Dey 1986) or that of permeability (e.g. Zoback and Byerlee, 1975).

In fact, Zoback and Byerlee (1975) showed that the effective stress coefficient for permeability of clay rich sandstone actually exceeds unity. These authors proposed a conceptual model where the low-compressibility quartz responds to the total stress, whereas high-compressibility clay in the pore space may be compressed by the pore pressure. If such clay is governing the permeability, it is easy to envision a coefficient higher than unity, for permeability, yet this would not impact similarly on the bulk volume compressibility. Finally, the volume change of porous media, i.e. the compressibility perspective, which is most relevant when utilizing eq. 1.2, is also discussed (Fatt, 1959; Van der Knaap, 1959). All these studies (Fatt, 1959; Van der Knaap, 1959; Todd and Simmons, 1972; Zoback and Byerlee, 1975; Christensen and Wang, 1985; Dey, 1986) discuss the effect of external and internal stress or pressure for porous sandstone.

The effective stress relation has also been studied for chalk (Teufel and Warpinski, 1990; Engstrøm, 1992; Gommesen et al., 2007; Olsen, 2007; Fabricius et al., 2008; Alam et al., 2009). Teufel and Warpinski (1990) performed laboratory experiments to determine the effective stress law for chalk, from both a permeability and compressibility perspective and reported poor agreement between the theoretical prediction and measured experimental data. Engstrøm (1992) presented a correlation between the Biot's coefficient and porosity based upon a limited dataset. These values of the coefficient were, however, based upon the very same theory that Teufel and Warpinski (1990) invalidated. One of the main challenges of high porosity soft chalk is its highly inelastic nature (Risnes and Nygaard, 1999). Biot (1941) listed

certain limiting assumptions for the effective stress concept, among these were the elasticity.

Recent studies on the effective stress concept related to chalk reveal a close relation between the effective stress coefficient calculated from dynamic moduli values and the cementation factor of chalk (Gommesen et al., 2007; Olsen, 2007). These studies showed that the dynamic effective stress coefficient could be used as a measure of the cementation degree for pure North Sea chalk. Further, Olsen (2007) showed that there existed a relationship between cementation and specific surface area of the bulk volume of chalk. Finally, Alam et al. (2009) addressed the difference between the effective stress coefficient measured from dynamic moduli values and the effective stress coefficient directly linked to compressibility, i.e. the effective stress coefficient measured from mechanical tests. They concluded that a coefficient calculated from sonic data predicts the effective stress coefficient for compressibility well with porosities around 30%, yet indicate that higher porosity (>40%) is less accurately predicted.

1.3 Chalk Compression

Reservoir compaction due to production is often caused by increasing load on the grains of the porous formation. In reality, this is a result of the decrease in pore pressure when the hydrocarbons are produced, as the effective stress in eq. 1.1 are increased by reducing P_P. Laboratory experiments should thus be loaded by depleting the pore pressure to properly mimic reservoir conditions (e.g. Shafer et al., 2008).

1.3.1 Uniaxial Strain Conditions

Basic rock mechanical relations simulating reservoir compaction are reviewed in paper III. This review covers the basics of uniaxial strain conditions, which is assumed to be a close representation of field behavior (Fjær et al., 2008). Paper III identifies the uniaxial strain modulus H, both in elastic and plastic region, and the relation between uniaxial strain and porosity. Also, the stress path when obeying uniaxial strain conditions, K_0, is defined as the ratio between the lateral and vertical stress changes (Fjær et al., 2008). K_0 is known to take varying values depending on the state of stress (Leddra et al., 1990; Loe et al., 1992; Jones, 1994), and may also be linked to the drained Poisson's ratio v_{dr} according to eq. 1.3 (e.g. Fjær et al., 2008):

$$K_0 = \frac{\nu_{dr}}{1-\nu_{dr}} \tag{1.3}$$

Chalk behavior during uniaxial strain conditions has been studied by several researchers (e.g. Heugas and Charlez, 1990; Leddra et al., 1990; Rhett, 1990; Loe et al., 1992; Jones, 1994; Risnes and Kleppa, 1996; Schroeder and Shao, 1996). Common for these studies is that chalk seems to fail in pore collapse when K_0 conditions are obeyed. On the other side, well test data from the Ekofisk Field suggest a constant stress path of 0.2 (Teufel and Rhett 1991). That study also presented experiments obeying constant stress paths, ranging from 0.17 to 0.33, which resulted in global shear failure. This agrees with the results by Risnes and Kleppa (1996). However Teufel and Rhett (1991) stated that pore collapse, despite global shear failure, took place in all their tests, in weak and volumetrically small domains in the bulk.

1.3.2 Elastic and Inelastic Chalk Behavior

Teufel and Rhett (1991) further discussed pore collapse in chalk as a hardening process. The authors relate such hardening and corresponding porosity reduction to increased material strength represented by expansion of the failure surface. Numerous failure surfaces or failure criteria have been proposed to capture the complexity of rock failure as a function of the principal stresses, σ_1, σ_2 and σ_3 (see e.g. Fjær et al., 2008). Such criteria typically describe projections onto a two dimensional stress plane or a failure space in a three dimensional principal stress space. In the so-called *q-p'* diagram used in paper III and VI, the principal stresses are represented by q, the generalized shear stress in eq. 1.4:

$$q = \frac{1}{\sqrt{2}}\sqrt{(\sigma_1-\sigma_2)^2+(\sigma_2-\sigma_3)^2+(\sigma_1-\sigma_3)^2} \tag{1.4}$$

and p', the mean effective stress in eq. 1.5;

$$p' = \frac{1}{3}(\sigma_1+\sigma_2+\sigma_3) \tag{1.5}$$

A schematic *q-p'* diagram is illustrated in Fig. 1.2(a). The shear failure line is intersected by an end-cap, which thus makes up the so-called yield envelope or yield surface. Chalk behavior within this yield surface is often referred to as being elastic. Further, when crossing the shear failure line, dilatant behavior is expected at low confining pressure. Crossing the end-cap results in

compactional pore collapse behavior. However, it should be mentioned that chalk does not behave fully elastic within this yield surface, as Risnes and Nygaard (1999) demonstrated inelastic behavior when stress cycles were performed well within the surface. This inelasticity could potentially be related to pore collapse in locally weak domains of the matrix at relatively high global shear stresses, as described by Teufel and Rhett (1991). Such local pore collapse could be related to breaking of coccoliths (Johnson et al., 1989), or frictional effects and sliding of grains (Risnes and Nygaard, 1999).

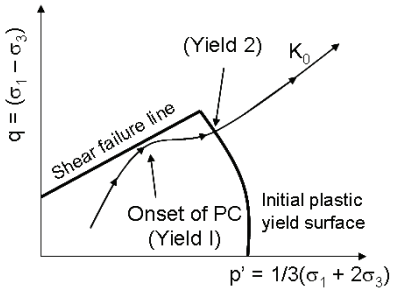

Fig. 1.2(a) Illustration of a yield envelope on a *q-p'* diagram; only compression behavior is included.

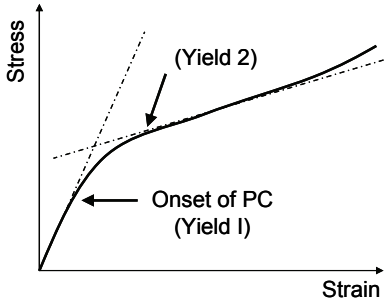

Fig. 1.2(b) Illustrated strain response under increased stress, including the definition of yield 1 and 2.

The yield surface is made up by yield points. By loading samples at different stress paths, yield will occur at various values of q and p'. These points make up the shear failure line and the end-cap. This is how the yield surface, from a practical perspective, represents the border between the elastic and plastic regime. The yield points are found graphically using a typical stress versus strain curve exemplified in Fig. 1.2(b). Havmøller and Foged (1996a) identified different methods of determining yield, as they define yield as a gradual process. Yield 1 in Fig. 1.2(b), is the onset of pore collapse and yield 2 corresponds to the onset of linear plastic deformation (Havmøller and Foged 1996a), which is really the end of the yielding process. Yield 2 or any average yield between these two extremes are less universal than yield 1 since they ignore a small amount of permanent strain before yield 2 is reached. Further, there is a human factor as well when deciding yield, hence it is important that the same procedure and judgment are used for all data compared. A schematic stress path of K_0 is included in Fig. 1.2(a), illustrating the approximate K_0 pattern reported by Leddra et al. (1990). The locations of yield 1 and 2 from Fig. 1.2(b) are also identified.

When a material is loaded beyond its elastic limit and therefore experience plastic compactional strains, the original elastic-plastic border is violated and not valid anymore. Proper theorectical description of such plastic rock

behavior, if loading is continued, requires work hardening functions and plastic flow rules (e.g. Charlez, 1991; Fjær et al., 2008). Alternatively, the 2-dimensional yield surface in Fig. 1.2(a) may be extended to three dimensions by introducing void ratio or porosity as the third dimension. These three axes are widely used to present soil behavior (e.g. Atkinson and Bransby, 1978; Fjær et al., 2008), and studies show that chalk may also be described by such plots (Leddra, 1990; Loe 1992; Jones; 1994).

This third dimension may also be represented by an expansion of the yield surface, and such expansion represents the evolving process of pore collapse and deformation. This process results in progressive decrease in porosity and a corresponding increase in rock strength (Teufel and Rhett, 1991). Such an expansion of the yield surface is, however, limited to the end-cap not including the shear failure line. Risnes et al. (1998) reported that strain hardening due to pore collapse only represents hardening towards further compression, since the material cohesion was greatly reduced by such failure. Accordingly, the shear failure line is not defined in the plastic regime since the material has lost cohesion. The shear failure line is here substituted by the critical state line which represents the ultimate state where large shear strains may occur at no change in shear stress (Fjær et al., 2008). Such updating of the yield surface according to porosity development resembles the concept presented by Havmøller and Foged (1996a), where the authors show end-cap update described as a function of the maximum stress seen for the chalk tested.

1.4 Time Dependent Deformation

Andersen (1995) defines three regions of deformation behavior; namely increased load, build-up of pore pressure including draining of this pore pressure (consolidation) and then finally creep. The two first phases, the increase in load and the resulted pore pressure response is strongly related and dependent on the rate of which the load was applied; i.e. load rate dependency. The nature of pure creep is a process less dependent on the loading. Powell and Lovell (1994) state that time dependent deformation of Ekofisk chalk comprise true secondary consolidation (here; creep), not affected by any pore pressure, thereby presume no consolidation. This review considers consolidation as a transitional stage between load rate effects and pure time dependent creep. In addition, the nucleus of failure concept presented by Andersen (1995) is reviewed as a possible additional explanation of the time dependency seen during loading.

1.4.1 Load Rate Dependent Nature of Chalk Failure

Several researchers have identified the load rate dependent nature of geomaterials (e.g. Bjerrum, 1967; De Waal 1986), and similar behavior has been reported for chalk (Smits et al., 1988; Ruddy et al., 1989; Andersen et al., 1992a). Basically, chalk deformation curves show that chalk deforms more per increased stress unit when loaded slowly compared to fast at laboratory rates. De Waal (1986) published the rate-type compaction model which identifies a material factor, the b-factor, describing the distance between the different deformational curves at different load rates in a typical stress versus strain plot. By the use of this b-factor, this model enables quantitative prediction of reservoir behavior from laboratory experiments.

Weak chalk is known to have small grains, relative to the pore size. Studies on chalk failure suggest a rather aggressive rearranging of this grain structure as chalk undergoes compactional deformation (Botter, 1985; Johnson et al 1989; Powell and Lovell, 1994). Chalk normally consists of a mixture of more or less intact coccoliths and calcite fragments, however, a SEM study by Johnson et al. (1989) revealed no surviving coccoliths in a mechanically compacted core. Powell and Lovell (1994) also reported break-ups of bioclasts, indicating that coccoliths break at far lower stress levels than the smaller fragments that are believed to obtain the stiffness of calcite.

The break-up of such bioclasts is regarded as the dominant cause of the pore collapse phenomenon in chalk (Botter, 1985). Alternatively, Powell and Lovell (1994) suggest that such break-ups of more or less intact bioclasts are less important in favor of simple grain displacement. They propose that grain sliding and rotation, so-called re-organization of the matrix, is responsible for most of the porosity loss observed when chalk is compressed along certain stress paths. Powell and Lovell (1994) also observed that this porosity reduction results in a homogenization of the matrix porosity, meaning that high porosity domains in the bulk volume experience more relative compaction than lower porosity domains. This is in agreement with the nucleus-of-failure concept.

Andersen (1995) describes the nucleus-of-failure concept based on observations showing that chalk has a weak microstructure. It is imagined that load is carried, on a microstructure level, by many sets of beams and arches. Chalk fails when these beams and arches are loaded above their limit. The beams and arches then yield, thus deformation occurs. The load will then be transferred to other support structures, most likely in the vicinity of the structure that just failed. It is thought that pore collapse is a cascade of such

transferring of load. In addition, it is thought that the following stress redistribution due to the structure reorganization takes time, since the chalk microstructure is not stable immediately after a change in load. This nucleus-of-failure model thus provides explanation for the time-dependent behavior of chalk when load is applied.

Andersen (1995) suggests that during steady-state loading, deformation is driven partly by the load directly and partly by the cascade failure: When the load rate is changed, the relation between these two contributing effects will change. For example, when the load rate is reduced, this cascade effect which in reality is a lagging effect will catch up while the amount of deformation driven by the load will be reduced. However, the relation will be regulated when the cascading adjusts to the new load rate. Alternatively, if loading is suddenly halted, the deformation is solely driven by this cascading effect. In this way, the nucleus-of-failure concept provides an explanation for the transitional behavior between the different virgin compaction curves defined by de Waal (1986). In both these examples, pure creep is neglected, i.e. it is solely deformation caused by a change in load that is considered.

This concept thus provides a supplementing explanation to the deformation often assumed to be caused by consolidation, i.e. the transient creep identified in Fig. 1.3. Consolidation is by conventional rock mechanics defined as the transient process where pore pressure equilibrium is re-established after a change in the stress (Fjær et al., 2008). When a saturated geomaterial is loaded in compression, the true stress state for the grains is influenced by the pressure of the saturation fluid inside the pores according to the effective stress principle in eq. 1.1. Most important is the pore pressure distribution throughout the matrix which obviously is dependent on the permeability, the thickness of the rock specimen and the drainage possibilities of the pore fluid. It is commonly believed within rock mechanics communities that such consolidation is responsible for some of the transient deformation after the loading is halted. Unfortunately, it is hard to differentiate between consolidation effects and the behavior described by the nucleus-of-failure concept. It is however clear that consolidation is not relevant for unsaturated or dry materials (Fjær et al., 2008).

1.4.2 Creep

Creep is often used as a collective term which covers all deformation that takes place when load increase is halted, i.e. deformation under constant load. However, the load is not constant if the rock is influenced by consolidation as

discussed in section 1.4.1. Fjær et al. (2008) differentiate between consolidation and creep of low permeable rocks or soil, and defines creep as time dependent deformation that occurs under constant stress. The traditional creep curve is illustrated in Fig. 1.3, showing the three common categories; primary or transient creep, secondary or steady state and last tertiary or accelerating creep. The first phase, the transient creep, is characterized by rapidly decreasing deformation rate as illustrated in Fig. 1.3. Fjær et al. (2008) state that when the applied stress is reduced to zero during this phase, the deformation is reversible, which clearly is associated with creep in a pre-yielded state.

The second phase is the steady state creep, where the rate is rather stable. The final creep state is the accelerating phase in Fig. 1.3. Accelerating creep leads rapidly to failure (Fjær et al., 2008), thus this final creep stage is more likely to occur for materials experiencing high shear stresses. Accelerating creep is to the knowledge of the author not yet reported for chalk. This is likely due to the high compressibility of chalk which favors a large amount of creep associated with porosity reduction. This tends to harden the chalk, according to Teufel and Rhett (1991). Such hardening expands the yield surface, which stabilizes the material as it can now tolerate more shear stress, i.e. not favorable for accelerating creep.

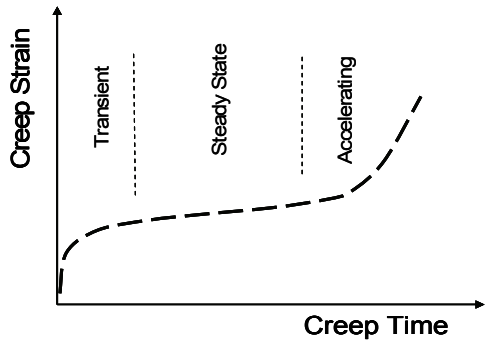

Fig. 1.3. Creep versus time, including the three stages of creep

Accordingly, creep may take place in both intact and failed materials. The mechanism responsible for creep is not fully understood. It is easy to envision that frictional sliding between the grains is responsible for creep in pore collapsed chalk. However, other mechanisms such as chemical and or mechanical rearranging of both the grains itself and the matrix structure may be contributing. Several authors have reported creep related to reservoir management and compaction of chalk, ranging from geological related pressure solution creep (e.g. Neugenbauer, 1974; Hellmann et al., 2002a;

Hellmann et al., 2002b) to production induced creep (Ruddy et al., 1989), chemical water weakening (e.g. Korsnes et al., 2006a; 2006b; 2008a) and impact of CO_2 injection in chalk (e.g. Madland et al., 2006).

Creep is known to follow a logarithmic behavior seen by the two first phases in Fig. 1.3, and empirical modeling of simple fitting models is a useful tool to visualize long term creep behavior. The advantage with empirical models is that they often reflect true rock behavior (Liingaard et al., 2004). However, these models apply only to experiments of similar boundary conditions; since well defined experiments are the basis for such models. These models provide a solution to engineering problems duplicated in laboratories. The simplest empirical creep predicting tool is perhaps the log-linear model used by e.g. Ruddy et al. (1989), where creep is described by the extrapolation of the constant slope commonly found for creep in a linear-log plot of strain versus time. However, Andersen (1995) mentions two main models for time dependent effect on chalk; namely the rate-type compaction creep model presented by de Waal (1986) and the extrapolation of the linear trend-line obtained when plotting the inverse of the creep-time data (Johnson et al., 1989)

1.5 Water Weakening

The type of pore fluid with which chalk is saturated is known to influence the mechanical strength, and such impact is clearly seen on the yield surface of chalk in a *q-p'* diagram (Risnes, 2001; Madland et al., 2002; Risnes et al., 2003). The dry and oil saturated chalk yield surfaces are much larger than the water saturated yield surface. This is referred to as the water weakening phenomenon and has been a topic for researchers for many years and still new findings uncover the details of this complex phenomenon. Gutierrez et al. (2000) gave a comprehensive review of the rather diversified work that had been done up to that point, mainly separating the proposed mechanisms in three categories; (I) physical effects, (II) physico-chemical effects and (III) chemical effects. In the first category (I), the physical mechanism most frequently discussed has been capillary pressure effects. These effects involve having a wetting and a non-wetting fluid which are immiscible and present in the pores at the same time. A capillary pressure within the pores of soils is an important aspect of the mechanical behavior of soils (e.g. Fjær et al., 2008). However, Risnes and Flaageng (1999) showed that the capillary forces could play only a minor role in chalk-fluid interaction and can not explain the mechanisms behind the water weakening phenomenon alone. The authors

suggested effects within the second category, physico-chemical effects (II), to be a dominating factor for the observed weakening. Physico-chemical effects is referring to stress corrosion (Hadizadeh and Law, 1991), adsorption of water on the chalk surface (Rhett, 1990) or the effect of water activity when changing the ion concentration of the pore fluid (Risnes et al., 2005).

The last category, chemical effects (III), has attracted increased attention the past years, however, it was already stated by Newman (1983) that the ionic composition of the brine injected into already aqueous saturated chalk would impact the mechanical properties. Madland (2005) systematically pointed out the important temperature dependence of the chemical water weakening of chalk. Heggheim et al. (2005) showed that aqueous brines not in equilibrium with the chalk would trigger dissolution which impacted the mechanical strength. This discovery by Heggheim et al. (2005) revealed a complex chemical picture as aqueous brines of various ionic concentrations were flooded through chalk cores (Madland et al., 2006; Korsnes et al., 2006a; Korsnes et al 2006b; Korsnes et al., 2008a; Madland et al., 2008; Zangiabadi et al., 2009). Common for these studies is that they are designed to emphasize any potential chemical effects, and the suggested mechanisms have so far been the substitution process and precipitation and dissolution processes.

1.5.1 Ion Substitution Hypothesis

Korsnes (2007) suggested that the chemical weakening of chalk subjected to seawater is due to a substitution process where calcium ions from the calcite grains are substituted by magnesium ions from the seawater. Studies had shown that seawater contains ions (calcium, magnesium and sulfate divalent ions) that are potential determining ions towards the chalk surface (Pierre et al., 1990; Strand et al., 2006; Zhang, 2006). The same ions seems to impact on the mechanical strength of chalk (Korsnes et al., 2006a; Korsnes et al., 2006b; Korsnes et al., 2008a). Korsnes et al. (2006a) documented that calcium ions have a higher affinity towards the chalk surface compared to magnesium ions when the system is at ambient temperature. However, as the temperature was increased, core flooding experiments showed that the magnesium ions present in seawater were able to substitute calcium ions from the chalk surface. Korsnes et al. (2006b) further showed that such ion substitution was dramatically influencing the mechanical strength of the chalk given that sulfate was present. That study presented mechanical tests of chalk samples flooded with seawater like brines at high temperature (130°C). Eventually, Korsnes et al. (2008a) mapped the temperature dependence of this chemical weakening mechanism, which is called *substitution of calcium with*

magnesium by the presence of sulfate (Korsnes, 2007). Finally, the direct link between the chemical mechanism and material strength was suggested to be the difference in size between the calcium and magnesium ions involved in the substitution (Korsnes et al., 2008a). It was further suggested that the substitution is required to occur at the intergranular contacts where the load is transmitted in order to affect the mechanical strength.

1.5.2 Dissolution and Precipitation Processes

Due to the differences in the ionic composition of the initial reservoir brine and seawater, the chalk formation and the injected seawater are not in chemical equilibrium. Equilibrium chemistry is a collective term which may include all different chemical reactions that happen in a closed system until thermodynamic equilibrium is achieved. Imagine that the pore fluid is allowed to reach equilibrium with the chalk matrix. If then new brine is introduced with a different ion composition, reactions would take place until a new equilibrium is established. Such chemistry was linked to the mechanical strength of chalk by Newman as early as 1983.

Newman (1983) concluded that compaction behavior of reservoir chalks depended on the water chemistry of the pore fluid. Since seawater seemed to have an adverse effect on the mechanical properties of chalks, formation water or an alternative chemical equivalent was suggested as injection fluid (Newman, 1983). Since then, rather few studies (see Madland, 2005) have been published dealing with water weakening of chalks from a pure chemical point of view. In a mechanical study by Heggheim et al. (2005) it was, however, concluded that a chemical mechanism involving dissolution and precipitation did play an important role when chalk cores were exposed to seawater like brines at 130°C. The experimental results were thus interpreted in terms of calcite dissolution and precipitation of anhydrite, $CaSO_4(s)$, and the chemical nature of the thin water film close to the intergranular contacts

Such a precipitation-triggered dissolution is somewhat similar to the concept of pressure solution proposed as a porosity reduction process during geological time. Pressure solution is the main responsible factor for induration of chalk in nature (e.g. Neugebauer, 1974). This phenomenon uses the fact that solubility of calcite is known to increase with pressure. Pore filling cement is therefore produced by dissolving the grains at the stressed intergranular contacts. This cement is supersaturated in the pore space where the pressure is less and will thus precipitate here. Pressure solution may also be present as part of the precipitation and dissolution process during core

flooding experiments. In fact, Hellman et al. (2002a; 2002b) presented experimental results of chemical water weakening and suggested the responsible mechanism to be pressure solution. However, the relative high porosities that are found in hydrocarbon North Sea chalk reservoirs indicates that pressure solution is arrested (Fabricius, 2003). Fabricius (2003) suggests two reasons that may arrest pressure dissolution: (1) reduced effective stress in the reservoirs and (2) adsorption of polar hydrocarbons on the chalk grains which may shield calcite from silicates. It is suggested that the presence of silicates is a pre-cursor for pressure dissolution in chalk, due to the absence of chemical compaction by calcite-calcite pressure dissolution (Fabricius, 2003).

1.6 Acid Stimulation

As mentioned in section 1.1, carbonate formations are acid stimulated by two different techniques; namely matrix treatment or acid fracturing. Matrix treatment is described simply as flooding the formation with acid at pressures below minimum principal stress. The acid will then enter the pore network and dissolve soluble compounds when reaching them. However, the most used technique for the Ekofisk field is as mentioned in section 1.1 the acid fracturing (Snow and Brownlee, 1989), where the acid is pumped at pressure higher than the minimum principal stress. Section 1.6.1 reviews the basic concept of acid fracturing. Section 1.6.2 focuses on the rock-acid interaction and etching pattern expected during an acid treatment.

1.6.1 Acid Fracturing

Hydraulic fracturing of wellbores has been a primary engineering tool for improving well productivity (e.g. Smith and Shlyapobersky, 2000). Such fracturing of wells may be performed to bypass near wellbore zones damaged during drilling, yet the most important reason for fracturing low permeable formations is to increase the inflow area. According to Darcy's law, eq. 1.6, the greater the flow area A the larger the fluid flow q;

$$q = \frac{kh}{\mu} \cdot \frac{\Delta p}{\Delta x}\left(\frac{A}{h}\right) \qquad (1.6)$$

As identified in eq. 1.6, other factors influencing q are the permeability k, the viscosity of the fluid μ, the height of the pay zone h and finally the pressure drop Δp over the investigated reservoir length Δx. A hydraulic fracture along

the axis of the well will significantly increase A, and such fractures are initiated by increasing the wellbore pressure above the fracturing pressure and thus creating tensile failure. The direction of the fracture depends on the stress field at the specific location and the fracture will stay open as long as the wellbore pressure exceeds the closure stress, which is associated with the minimum horizontal stress (e.g. Tjetland et al., 2007).

The challenge is to keep the fracture open as the pressure in the fracture drops below the closure stress in order to create drawdown in the well. Acid fracturing is an alternative to propped fracture where the fracture is kept open by proppants. In the case of acid fracturing, the acid is intended to etch the walls of the fracture and thereby create patterns making the two matching fracture walls highly irregular with respect to profile, roughness and shape. When the stimulation is completed and the well pressure is drawn down and the well starts producing, the fracture will close. Conductivity is ensured if the two walls do not fit perfectly together as the fracture close

1.6.2 Wormholing or Cavity Creation

The mineralogy of reservoir and outcrop chalks varies in terms of clay and silica content as described in section 1.1.1, but common for all chalks is the high calcium carbonate content, typically >95 wt% (Hjuler, 2007). When 15 wt% concentration hydrochloric acid is pumped into chalk formations, according to Snow and Hough (1988), it will react instantaneously with the calcite and form aqueous calcium chloride, carbon dioxide and water, according to eq. 1.7.

$$CaCO_3 + 2HCl \leftrightarrow CaCl_2 + CO_2 + H_2O \qquad (1.7)$$

Robert and Crowe (2000) state that the solid-liquid reaction in excess of hydrochloric acid is complete and irreversible and that the byproduct, calcium chloride, is highly soluble in spent acid, i.e. no risk of reprecipitation. However, Mumallah (1991) emphasised that experiments should be conducted fluid pressure of 3000 psi (~20 MPa) or more to keep the carbon dioxide dissolved in the water. Mumallah studied different influencing factors for the reaction rate between hydrochloric acid and chalk, and concluded that the reaction of hydrochloric acid with chalk is characterized as mass transfer limited, since the chemical reaction is instantaneous compared to the mass-transfer steps (Mumallah, 1991).

Due to the high reaction rate, the acid tends to etch preferred pathways, often called wormholes, in the matrix (e.g. Hill and Schechter, 2000). The acid is apparently following local high-permeability streaks rather than progressing through the formation as a uniform front. As soon as one pathway is enlarged, it will be preferred with fresh acid, which will follow an open pathway rather than the low permeable pore-channel network. Acid is etching the walls constantly; hence this pathway will grow faster and faster compared to the other matrix flooded areas. This process will continue until one or a few such pathways have enough flow-capacity to transmit all injected acid. Then it may be suggested that the matrix is basically not flooded at all. All acid is flooding in the wormhole or acid channel, which will be further enlarged and extended.

Acid fracture conductivity, as described in the previous section, is dependent on the acid etched pattern, given that the acid forms fingers much similar to the wormholing concept along the fracture wall. Gel is therefore pumped in front of the acid to prevent the acid from leaking off into the formation (Snow and Hough, 1988). This assumption of differential etching on the fracture wall to maintain the fracture conductivity is founded in experiments carried out on low porous carbonate rock rather than soft high porosity chalk. The increased production achieved has proven to be rather short lived (Snow and Brownlee, 1989; Montgomery et al., 2005). The classical interpretation has thus lately been challenged, suggesting that a huge cavity is actually created rather than the fracture fingering.

The rock mechanical response of such a cavity during production has been experimentally investigated by performing loading experiments on thick wall cylinder-cores from Ekofisk, (Montgomery et al., 2005). These results show that shear failure, in the form of `shear-bands`, is developed for the particular chalk material and loading conditions used. The creation of such fracture bands will enhance porosity and permeability when the material dilates which explains some of the increased productivity experienced after acid stimulation, in addition to increased downhole radius. One of the reason why productivity increases is short lived (Snow and Brownlee, 1989; Montgomery et al., 2005) might be related to the closure of these induced `shear-bands` around the cavity when the stresses get too high and the material may start to be contractive instead of dilative. The way such potential acid created cavities deform depends on initial cavity geometry, stress path (Malmin, 1998) and the rock properties, e.g. the porosity. If the creation of such a cavity is realistic, it could also lead to liner failure due to non-uniform loading (Pattillo and Kristiansen, 2002). Indeed, liner deformations have been seen in the Ekofisk field (Montgomery et al., 2005).

2 Objectives

Subsurface technologies such as petroleum geomechanics often rely on indirectly acquired data gathered from seismic and well logs. The only direct measurements available for static mechanical properties are those obtained on core material tested in laboratories. The closer to reality the controlled laboratory conditions become, the better is the representation of the field.

The petroleum reserves in the southern part of the North Sea are often found in chalk formations. These chalk reservoirs are generally described as geomechanically weak with high initial porosity. The matrix permeability of chalk is low (1-10 mD), but the formations are usually highly fractured, which makes the hydrocarbon production commercial. The geomechanical complexity of the chalk reservoirs makes the mechanical response to reservoir management difficult to forecast. The scope of this thesis has been to approach realistic reservoir conditions in the triaxial cells at the laboratory, and the relevant reservoir challenges addressed are principally related to five main categories:

- Experimental challenges regarding the effective stress relations
- Time and rate effects during depletion close to in-situ conditions
- Seawater impact on creep close to in-situ conditions
- Basic mechanisms for chemical water weakening
- Effect of acid injection as a function of various chalk properties

Series of rock mechanical experiments have been performed under conditions as similar as possible to normal reservoir operations for the Ekofisk and Valhall Fields. By “reservoir conditions” mean relevant temperature and pore fluid saturation, realistic stresses, which includes high pore pressure, lateral and overburden stress and stress path, and that the actual loading is performed by depleting the pore pressure. The goal has thus been to increase the applicability of fundamental laboratory research to the petroleum operators.

3 Materials and Methods

3.1 Core Material and Preparation

Outcrop chalk from four different locations together with chalk from a North Sea reservoir has been used as core material for the experiments. These chalks have been used for various tests as reflected in section 3.1.2 which describes the different fluids used during testing. Finally, the cores are prepared for testing as described in section 3.1.3.

3.1.1 Sample material

The majority of this work has been carried out using core material from the open quarry in Fig. 3.1, called Sigerslev Kridtbrud, at Stevns Klint near Copenhagen, Denmark. This chalk is throughout this thesis called Stevns Klint chalk, and used for experiments in all papers except paper VII. Stevns Klint is characterized as Maastrichtian or late Cretaceous of age (Håkansson et al., 1974). Further, this chalk is famous for its very high porosity, sometimes above 50%, and low non-carbonate content (<1%) (e.g. Håkansson et al., 1974; Hjuler, 2007). Another chalk of Maastrichtian age, the Aalborg chalk, from an open quarry at Rørdal close to Aalborg in Denmark, is used in paper VII. This high porosity chalk (~45%) is known to have a higher non-carbonate content than the Stevns Klint chalk, and Hjuler (2007) reports ~6%, mostly silicates in the form of quartz and opal-CT. Liège chalk, collected from an open quarry at Lixie, near Liège in Belgium is used in papers V and VII. This chalk has a porosity around 42%. In some literature this chalk is referred to as Hallembaye chalk (e.g. Håkansson et al., 1974; Hjuler, 2007), and Hjuler (2007) reports a non-carbonate content, mostly consisting of quartz and clinoptilolite, of roughly 1.5%.

For the purpose of testing lower porosity material, upper Cretaceous chalk from Niobrara, West-Kansas, US (Hattin and Cobban, 1977) was prepared and tested. As for the Stevns Klint chalk it is known to have a high calcite content, >99% (Caldwell, 1992). The matrix consists of coccoliths as for the Maastrichtian chalk as seen in Fig. 1.1. Low (25-27%) and medium porosity (39-44%) Kansas chalk is used in paper VII, and ~37% porosity Kansas chalk is used in papers I, III and VI.

3.1.2 Fluids

Nine different types of fluids have been used to either clean, saturate or flood the samples and provide pore pressure. Table 3.1 lists the different fluids with their abbreviations. The purpose of the fluids used is also briefly mentioned. More details are found in the respective papers where the tests are presented. The characteristics of each fluid, such as chemical composition are also specified.

Table 3.1. Various fluids used to either clean, saturate or flood and provide pore pressure

Fluid	Purpose	Characteristics
Distilled water *DW*	Used to clean cores and provide pore pressure. Used in paper I, III, IV, V, VI and VII	Water that has all of its impurities removed through distillation
Artificial Valhall Brine *AVB*	Used to simulate initial connate water. Used in paper III, IV and VI	NaCl – 57.70 g/l, $NaHCO_3$ – 0.78 g/l, KCl – 0.40 g/l, $MgCl_2 + 6H_2O$ – 1.58 g/l $CaCl_2 + 2H_2O$ – 4.26 g/l
Synthetic seawater *SSW*	Used to investigate effects of water weakening. Used in paper II, V and VI	NaCl 23.38 g/l, Na_2SO_4 – 3.41 g/l $NaHCO_3$ – 0.78 g/l, KCl – 0.40 g/l, $MgCl_2 + 6H_2O$ – 1.58 g/l $CaCl_2 + 2H_2O$ – 4.26 g/l
Magnesium chloride brine $Mg_{0.109}$ $Mg_{0.218}$	Used to isolate the effect of magnesium on water weakening. Used in paper V	As indicated by the abbreviations, two concentrations are used; 0.109 M and 0.219 M
Sodium chloride brine $Na_{0.657}$	Used to isolate the effect of sodium on water weakening. Used in paper V	As indicated by the abbreviation, 0.657 M used as concentration
Hydrochloric acid *HCl*	Used to simulate acid stimulation. Used in paper VII	HCl mixed with distilled water with concentrations of 3.5, 7.0 and 15.0 wt% used
Ethylene glycol *EG*	Used to investigate fluid dependency on pore pressure response. Used in paper I and IV	Mixable in water, ethane-1,2-diol with chemical formula; $HOCH_2CH_2OH$
Hepthane *HP*	Used as initial oil-saturation for cores simulating reservoir conditions. Used in paper III, IV and VI	A non-polar solvent, a straight-chain alkane with the chemical fomula; $H_3C(CH_2)_5CH_3$
Kerosene *KE*	Used as pore fluid in the cores tested at CoP-BTC. Used in paper I, III, IV, VI	Mixture of carbon chains, typically 6 to 16 carbon atoms per molecule, density of 0.78-0.81 g/cm^3

3.1.3 Core Preparation, Cleaning and Saturation

Outcrop chalk samples are collected from the open quarries in blocks with typical size of 0.1-1 cubic meters. Test samples are then cored, machined and cut to the appropriate dimensions. In this work, core diameters have varied from 1 inch up to 1.5 inches. Further, the rule of thumb determining the appropriate core length demands a length roughly twice the diameter (Fjær et al., 2008). These requirements have been met for the cores used in this study.

Fig. 3.1. Picture taken from the open quarry outside Copenhagen, Denmark.

The quarry at Stevns Klint in Fig. 3.1 is located close to the sea. Contamination of salts in the pores is thus likely to occur as ions accumulate during the constant wetting and drying of the formation by the waves, wind and sun. In fact, previous work has detected various ions initially present in the core material. Consequently all cores subjected to chemical investigations, except the reservoir samples, are cleaned by flooding some pore volumes of distilled water (Puntervold et al., 2007).

The porosities are determined by simple weight analysis. The sample weight, after drying above the boiling temperature of water, is regarded as the dry-weight of the cores. The samples are then saturated by distilled water using vacuum (~0.06 kPa), and this new weight is regarded as the weight of fully saturated cores. The porosity determined by using these two weights is the effective porosity. Also, when saturating the cores with specific brines or fluids, a similar procedure using vacuum is used.

Porous plate apparatus was used for preparing cores with low initial water saturation to simulate the original connate water of the reservoirs. Cores saturated with artificial Valhall brine *AVB* are connected axially on a porous plate by chalk paste to ensure continuous capillary contact between the two porous media. The brine is then drained out of the cores, through the porous plate by gradually increasing the pressure of water-saturated N_2-gas towards 1.4 MPa. This method is intended to result in uniform residual brine saturation. This final saturation is believed to depend on permeability and porosity of the cores and the drainage time and pressure of the N_2-gas. The two reservoir cores were prepared slightly differently from the outcrop material. The bulk volume was measured by mercury immersion and subsequently the porosity was measured by a helium porosity meter. Finally, the initial brine saturation, using a brine equivalent to *AVB*, was achieved by the use of a centrifuge.

3.2 The Triaxial Cell

The results and discussion in this thesis are based on experimental data acquired by the use of a hydraulically operated triaxial cell. Fig. 3.2 illustrates schematically a standard triaxial cell used for most of the tests. This sub-chapter introduces the basics concerning its design and demonstrates how the cell may be used for the rather diversified range of tests performed. A more comprehensive description of the triaxial test and its advantages and limitations may be found in the textbook of Bishop and Henkel (1962).

3.2.1 Cell Design

The test cell in Fig. 3.2 is designed without an external load frame. The axial as well as the lateral load is applied hydraulically by high pressure/low volume piston pumps. The core is mounted between two steel cylinders, marked I in the illustration, the lower one fixed on the bottom base of the cell. A steel skirt makes up the confining chamber surrounding the sample, as seen in Fig 3.2, where the core is located in the middle inside a pressure vessel. This pressure vessel is completed when the axial piston assembly is mounted on top of the steel skirt and the bolts are made up.

Axial load is applied by this piston assembly, marked with II. This hydraulically operated piston is moved downwards when the pressure in the

upper piston chamber (see Fig. 3.2) is greater than the pressure in the lower piston chamber, and vice versa. The piston assembly is in the lowermost position in the figure and the lower piston chamber is thus small. The axial piston assembly is balanced in the sense that the confining stress is applied axially; the fluid in the confining chamber is allowed to move up inside the piston and into the chamber for balancing confining pressure (see Fig. 3.2). Due to this particular design, the pump in the axial circuit only provides the additional pressure beyond the confining pressure. It should also be mentioned that the additional axial pressure includes any friction along the piston movement, which is measured individually for each test.

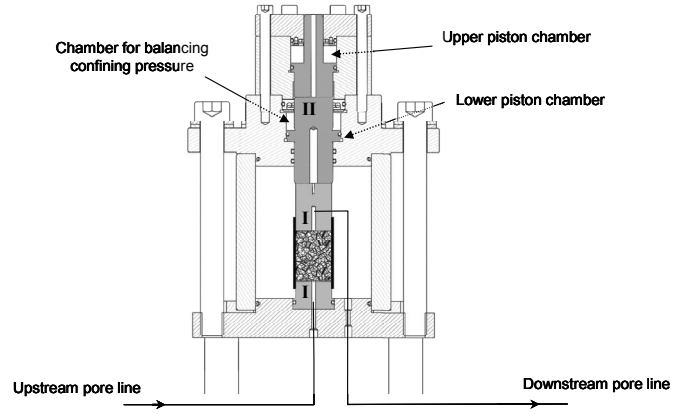

Fig. 3.2. Triaxial cell, highlighting the pore line and the axial piston assembly

The steel cylinders marked with I in Fig. 3.2, between which the core is mounted determines the samples' diameter. Core deformations are measured by two different systems. The movement of the axial piston is measured by an outside linear voltage displacement transducer (LVDT) (±0.05 mm). The axial strain of the sample is thus measured indirectly, as this LVDT follows the piston movement externally and measures the entire deformation in the vertical axis. However, it has been shown that compression of the axial piston assembly may be disregarded compared to the accuracy of the LVDT and the fact that chalk deformation is an order of magnitude greater than steel. Lateral displacement is measured by the use of a chain surrounding the core connected to an extensometer for detection of any change of the circumference. The cell is also equipped with a heat regulating system allowing test temperatures up towards 150 ±0.2 ºC.

The test core is a closed system, separated from the confining fluid by a sleeve, indicated by the thick black lines around the sample in Fig. 3.2. The

steel cylinders (marked I in the illustration) enclosing the core on the top and bottom are perforated allowing flooding possibilities. The upstream pore line is connected to the injection system, which by use of a high pressure piston pump and piston cells allows flooding of various brines. The downstream pore line is either open to air, connected to a simple back pressure regulating system (BPR-system), which maintains stable pore pressure (±0.1 MPa) or connected to a pump which serves as a back pressure regulator and allows testing at high values of pore pressure.

3.2.2 The Hydrostatic Test

Testing at hydrostatic or isotropic conditions is to expose a specimen to an increased stress state with an isotropic stress field, i.e. equal stresses in all directions. The test is mainly performed to determine the bulk modulus K_b of rocks (and of grains by testing "unjacketed"), to measure hydrostatic yield or to perform the initial phase in a typical triaxial test (Fjær et al., 2008). By using the cell in Fig. 3.2, the test is performed by increasing the confining pressure while recording any deformations on the sample. However, since the axial deformation is measured via the piston assembly as described in section 3.2.1, it consequently follows that the piston needs to be in contact with the sample. The challenge is to overcome the friction, but at the same time not add extra load to the core. The hydrostatic test, performed in the cell illustrated in Fig. 3.2, is therefore considered quasi-hydrostatic, with an additional axial load typically in the range of 0.1-0.3 MPa.

Scatter is associated with laboratory data, also when it comes to rock mechanical chalk data. However, less scatter has been seen on the hydrostatic yield as well as creep obtained following the hydrostatic load phase, thus this test has proven quite useful when investigating the effect of various brines on the mechanical strength of chalk.

In this work, the hydrostatic test is used in paper II, IV and V.

3.2.3 The Isochoric Test

The isochoric test is, as presented by Charlez (1991), a way of experimentally determining the effective stress coefficient α from a bulk volume perspective. Basically, the isochoric test involves ramping of the confining and pore pressure and at the same time maintaining isochoric conditions ($\Delta\varepsilon_v = 0$). This

is ensured by regulating the confining and pore pressure relative to each other. When doing this, α is given by eq. 3.1;

$$\Delta\varepsilon_v = \frac{3}{K_b}\left(\Delta\sigma_{iso} - \alpha\Delta P_P\right) \tag{3.1}$$

because isochoric conditions ($\Delta\varepsilon_v = 0$) reduces eq. 3.1 to eq. 3.2:

$$\alpha = \frac{\Delta\sigma_{iso}}{\Delta P_P} \tag{3.2}$$

σ_{iso} in eq. 3.1 and 3.2 represents isotropic stress, thus the starting point for the isochoric test is hydrostatic conditions, section 3.3.1. Further, eq. 3.1 and 3.2 assume ideal homogeneous deformations, i.e. $\varepsilon_i = \varepsilon_j = \varepsilon_k$ and ε_v is the volumetric strain. K_b represents the bulk modulus

In this work, the isochoric test is used in paper I.

3.2.4 The Uniaxial Strain, K_0, Test

This test is performed in such a way that the core only experiences deformation in one axis. The test is called the Odeometer test when it is performed in an Odeometer cell. In that case, samples are placed inside a solid, undeformable cylinder and compressed vertically, which enforce uniaxial deformation. Alternatively, as in this work, the K_0 test may be performed in a triaxial cell. Here, the lateral stress, i.e. the confining pressure, needs to be adjusted to maintain constant diameter of the core while compressing with the axial piston assembly in Fig. 3.2. Executing a uniaxial strain test in the cell shown in Fig. 3.2 is not straight forward. The particular design ensuring that the confining pressure is balancing the piston is a challenge in this context. Whenever the confining pressure needs to be adjusted to maintain constant diameter, the axial load will consequently be influenced. Due to this, it is not recommended from a practical point of view to run uniaxial strain tests by increasing the axial stress from zero axial stress. The core might require more adjustment in terms of confining pressure than feasible.

However, the uniaxial strain test is feasible on the triaxial cell in Fig. 3.2 when testing at advanced conditions, similar to the tests close to reservoir

conditions in this work. When loading the sample by depleting the pore pressure while the axial load is constant there will always be sufficient regulating margin in terms of confining pressure. The challenge is to maintain constant axial load due to the particular design of the cell. To run this smoothly, a quick and responsive pump with capability to deliver and receive fluids is needed as well as software that could send the appropriate piston pressure P_{piston} to the pump according to eq. 3.3.

$$P_{piston} = \frac{P_{set} - P_c \times (1 - frictionfactor)}{areafactor} \tag{3.3}$$

where P_{set} is the constant axial load and P_c the confining pressure. The friction factor mentioned in section 3.2.1 is found experimentally by running the piston at different confining pressures, i.e. a factor dependent on P_c. The area factor compensates for any inconsistency between the area P_{piston} is allowed to act on and the cross-section of the core itself.

In this work, the uniaxial strain test is used in paper III, IV and VI.

3.2.5 Creep

Creep, as defined in section 1.4.2, has been tested for cores following both the hydrostatic test (3.2.2) and the uniaxial strain test (3.2.4). Hydrostatic creep has been conducted by simply maintaining the stresses while monitoring the resulting deformations with time. For the uniaxial strain creep, however, the axial stress was maintained while the lateral stress was regulated to avoid any lateral strain.

Creep has been investigated in paper III, IV, V and VI.

3.2.6 Acid Stimulation

The flooding possibility in the triaxial cell was utilized for acid stimulation tests. Cores were installed and initial confining pressure was established similar to performing a hydrostatic test. 50 °C was established to simulate a near wellbore situation, which is regarded as somewhat cooler than the reservoir itself due to massive water injection. Acid was then injected at relatively high rates (up towards 10 ml/min).

The challenge was to provide enough confining pressure to prevent leakage of acid into the confining bath. The high rate flooding resulted in a huge pressure drop over the core of several MPa. This needed to be matched by the confining pressure. Simultaneously, the intention was to maintain the core as intact as possible because the cores were to be visually inspected afterwards.

The core setup was also special for the acid stimulation experiments. In order to experimentally emulate what takes place in the field, three different core setups were developed: An intact core setup simulating intact formation, a split core simulating a fractured well, and a split core with an end-plug, simulating the transition from fracture to matrix. The split or fracture was always in the same axis as the flooding direction.

In this work, the acid stimulation test is used in paper VII.

4 Fundamental Rock Mechanical Investigations

4.1 The Effective Stress Relation

The background for studying the effective stress relation introduced in section 1.2 originates from incidental observations obtained when ramping up the pressures in order to reach in-situ reservoir conditions in the triaxial cell. Fig. 4.1 demonstrates these observations. The grey dotted curve represents the total isotropic stress versus pore pressure. From the initial state of 3 and 1 MPa, the total isotropic stress and pore pressure are increased towards 27 and 25 MPa, respectively. Even though the 2 MPa differential stress is maintained, the core accumulates 7‰ axial strain, indicated on the x-axis.

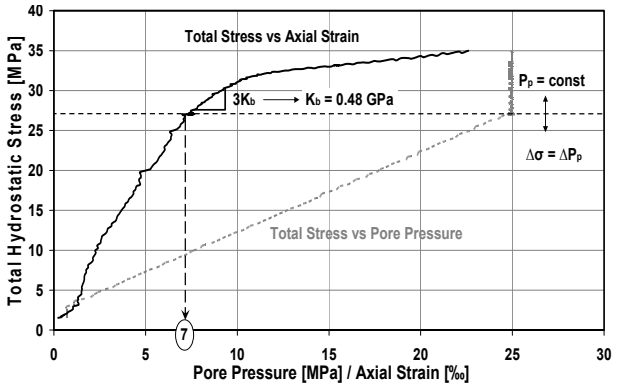

Fig. 4.1. Simultaneous increase of total isotropic stress and pore pressure for a Stevns Klint core with porosity of 48.9%. The total stress plotted versus axial strain and pore pressure.

As seen from the black solid curve in Fig. 4.1, the slope changes as the total isotropic stress is further increased from 27 MPa while the pore pressure is kept constant. As reported in paper I, and indicated in Fig. 4.1, the bulk modulus K_b is equal to 0.48 GPa from this slope. Knowing that the modulus values are the inverse of the compressibility, K_b may be used in eq. 1.2 to estimate α, assuming that the solid modulus K_s (= C_s^{-1}) for calcite equals 74 GPa (e.g. Fjær et al., 2008). The value of α then equals 0.99, i.e. close to 1. According to such a high α, the simultaneous increase of the total isotropic stress and pore pressure is apparently representing a state of constant effective stress, so the 7‰ deformation accumulated is highly unexpected. Similar observations were seen for several cores and on this background it was decided to investigate the effective stress relation in more detail. This

investigation is performed from two perspectives, i.e. from a compressibility (paper I) and a material strength point of view (paper II). Knowing that strain and yield is a result of a change in load; they may both serve as indicators of effective stress.

4.1.1 The Compressibility Perspective

Charlez (1991) presented an experimental program for measuring the effective stress coefficient by performing the isochoric test, as described in section 3.2.3. The isochoric test excludes time dependent strain and assumes incompressible grains, which is appropriate for the tests in paper I which are short term experiments *<100 min* and the calcite grains obtain a high solid modulus K_s *- 74 GPa* (e.g. Fjær et al., 2008). Fig. 4.2 shows an example from paper I, where a core is tested according to the isochoric test program. The part of the test where the effective stress coefficient is measured is the period from 80 to 160 minutes. The total isotropic stress is increased from 20 to 40 minutes to establish a regulating margin as indicated in the figure. This margin is compromised in the phase from 80 to 160 minutes where the bulk volume is kept constant. The volumetric strain is included, and as observed it barely fluctuates from 0 to 0.1‰ volumetric strain, Fig. 4.2.

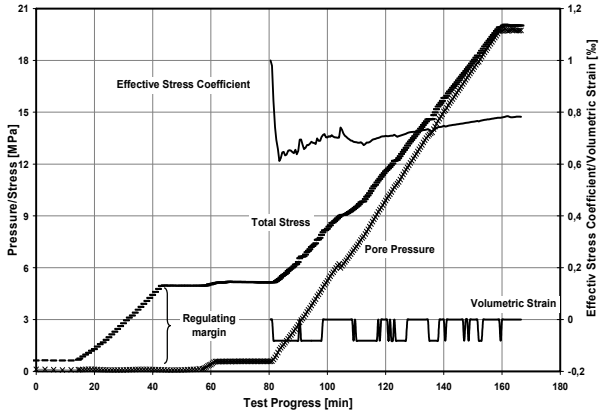

Fig. 4.2. Water saturated Stevns Klint core tested according to the isochoric test program. Initial differential stress of 5 MPa at 80 min (regulating margin).

The effective stress coefficient is calculated according to eq. 1.1 in section 1.2, and σ is in Fig. 4.2 represented by the total stress curve, P_P is the pore pressure curve. The effective stress, σ' in eq. 1.1, equals the regulating margin and is, according to the concept of the isochoric test, constant as long as $\Delta\varepsilon_{vol} = 0$. By using these identified factors eq. 1.1 produced the curve for the

effective stress coefficient in Fig. 4.2. It mathematically starts at 1, yet rapidly drops towards 0.6, before it converges throughout the test towards 0.8. As reported in paper I, chalk cores with porosities ranging from 36.80% to 47.56% were tested. The case in Fig. 4.2 represented the tests performed in the elastic regime. The regime is determined by the amount of regulating margin. The average effective stress coefficient for Stevns Klint cores saturated with distilled water roughly converges from 0.62-0.78 in the elastic phase. The equivalent values from the plastic regime, where the regulating margin was set to 15 MPa, were found to be reversed as they converge downwards on average from 0.76-0.58. Surprisingly, the core with the lowest porosity obtained the highest value, going from 0.89 – 0.93. This core was saturated with kerosene. The effect of the saturating fluid seems, however, not to be significant as a high porosity (47.56%) Stevns Klint core, also saturated with kerosene, obtained a lower value of α (0.70-0.89).

4.1.2 The Strength Perspective

The isotropic or hydrostatic yield strength of chalk is determined according to Fig. 1.2(b) in section 1.3. Mechanical parameters acquired under isotropic conditions are shown to be rather consistent and comparable (e.g. Korsnes et al., 2008b) so on this basis it is argued that the yield strength is a stable indicator of the effective stress level. Fig. 4.1 may be used to describe the program for the cores tested. After the phase where the total isotropic stress and pore pressure is simultaneously increased with a constant window of 2 MPa difference stress, the window is increased up to 10 MPa. This loading caused all cores to fail in pore collapse mode, i.e. hydrostatic yield.

The test in Fig. 4.1 is performed with a pore pressure of 25 MPa and the total isotropic stress was increased to 35 MPa. Yield for this core was initiated around 31.5 MPa total isotropic stress, equivalent to 6.5 MPa differential stress. This was repeated at different levels of pore pressure, ranging from 0.7 to 25 MPa. Each of the 12 data points in Fig. 4.3 represents the yield point of an individual experiment similar to the test in Fig. 4.1. The differential stress and the total isotropic stress for each yield point is plotted on the y- and x-axis, respectively. Fig. 4.3 indicates a trend suggesting that the differential yield is not affected by the increase in total isotropic stress. It should be mentioned that the lowest point of differential yield, the core with porosity of 49.7 tested with 15 MPa pore pressure, sticks out as scatter. All other cores yield around 6.25±0.75 MPa differential stress.

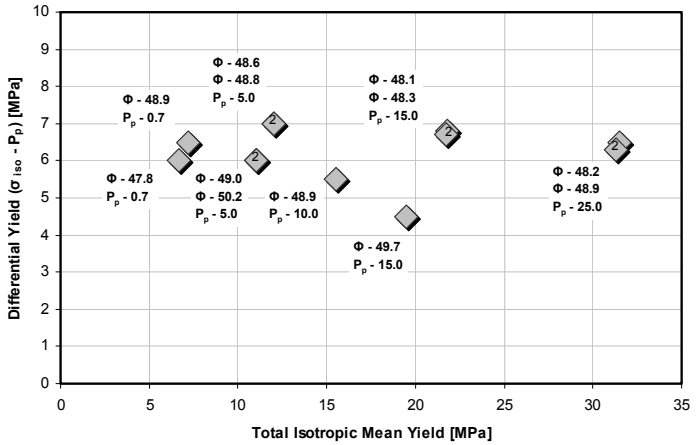

Fig. 4.3. Yield strength as a function of total isotropic stress on the x-axis versus differential stress, i.e. the difference between the total isotropic stress and the pore pressure, on the y-axis.

The results in Fig. 4.3 suggest an effective stress coefficient α close to unity. Paper II argues the data in Fig. 4.3 would produce a declining trend if α was a value lower than unity. This argument utilizes the fact that the values on the y-axis are the differential stress. The differential stress consequently decreases if the effective stress is kept constant and the pore pressure increases given a case with $\alpha < 1$. Accordingly, if α really was approximately 0.75 (paper I), the trend in Fig. 4.3 should be declining. Since it is showing a more or less horizontal trend, the effective stress coefficient is found close to unity from the strength perspective.

4.1.3 Compressibility and Strength Perspectives in Combination

The core material used for to study the effective stress relations is limited to high porosity outcrop chalk, (36-50% porosity). Conventional assumptions state that α will take lower values with lower porosity and higher strength, according to eq. 1.2. An experimental study on reservoir chalk with 15-36% porosity concluded that α is decreasing with decreasing porosity (Teufel and Warpinski, 1990). The measured values for α in paper I contradict these results by the fact that the core with the lowest porosity shows the highest value of α.

Alam et al. (2009) performed an experimental study measuring the effective stress coefficient and the Biot's coefficient for Valhall chalk. The study defined the effective stress coefficient similar to the coefficient from a compressibility perspective in section 4.1.1, while their Biot's coefficient is

defined as the dynamic effective stress coefficient calculated from density and sonic velocity data. Alam et al. (2009) found that chalk around 30% in porosity obtains similar effective stress- and Biot's coefficient. However, poor agreement was found when investigating higher porosity chalk (~40%). This may explain why the lowest porosity core in paper I obtained the highest coefficient. Alam et al. (2009) reports an effective stress coefficient as low as 0.75 for a 40% porosity core, which agrees with the values measured for the high porosity Stevns Klint cores in paper I.

Paper I excluded time dependency by performing rapid experiments and by varying the load rates, and rather discussed this inconsistency as effects of inelasticity. Teufel and Warpinski (1990) furthermore concluded that nonlinearity invalidates most theoretical and mechanistic models, which also becomes obvious from this present study. The effective stress theory is based on the assumption of elasticity and linearity of stress-strain relations. Years of research on chalk reveals that these relations only to some extent apply for chalk (e.g. Risnes and Nygaard, 1999).

Risnes and Nygaard showed that quasi elastic behavior of chalk resulted in permanent strain that accumulated during repeated stress cycling, even in a pre-yield state of the material (1999). It could be argued, as illustrated in paper II, that simultaneously ramping of the total isotropic stress and pore pressure is on infinitesimal time scale experienced as many small load cycles. Perhaps such infinitesimal plastic contributions of strain might explain the unexpected strains demonstrated in Fig. 4.1. Since α found from a strength perspective is close to unity, this inelasticity does not seem to affect the yield strength of the material.

Zoback and Byerlee (1975) suggested a dual compressibility concept with independent compressibility of the sand and the clay for a Berea sandstone that displayed a strange permeability behavior. A similar concept may be proposed for chalk. A SEM investigation suggested a rather aggressive rearranging of the grain structure indicating that the more or less intact coccoliths were crushed as chalk underwent deformation (Johnson et al., 1989). Consequently, if coccoliths break at far lower stress levels than calcite, chalk may be described as a dual compressibility system; different compressibilities of the calcite grains and of the coccoliths. Thus a similar conceptual model may explain some of the inconsistency and inelasticity observed during simultaneously ramping of the confining and pore pressure.

4.2 Time Dependency during Loading

Time dependent behavior during loading as introduced in section 1.4 has been demonstrated for chalk in paper III and IV. This subchapter reviews load rate effects on deformation and discusses the results in terms of consolidation or nucleus-of-failure effects. In addition, creep results are covered.

4.2.1 Determination of the Material Constant *b*

The intention of using alternating load rates for SKS 11, K 19 and R 26 in paper III was to detect potential load rate effects and determine the b-factor required to utilize the rate-type compaction equations of the de Waal model (de Waal, 1986). According to this concept, a material will deform along the virgin compaction curve of that specific load rate. If the load rate is varied, the stress and deformation data will transition to another virgin compaction curve dependent on the new load rate. The b-factor is a material constant that describes the distance between these curves. For SKS 11, the b-factor was found equal to 0.061, while for both K 19 and R 26, the b-factor was 0.040. It is worth mentioning that a similar b-factor was obtained for the Kansas and reservoir material, which may suggest that the Kansas chalk is an appropriate reservoir analogue for that particular reservoir. Likewise for the Stevns Klint sample, that showed similar b-factor as reservoir chalk from the Valhall field; 0.065 according to Andersen et al. (1992b). This observation supports the findings by Hjuler (2007) who suggested Stevns Klint to be a suitable geomechanical analogue to the Valhall Field due to modest calcite redistribution and poorly connected particles.

4.2.2 Porosity versus Load Rate Dependency

In paper III, the series of Stevns Klint cores depleted at conditions close to the Valhall Field is depleted with two different rates; 1 and 31 MPa/day. Fig. 4.4 shows the depletion response in a typical stress-strain plot. As seen, SKS 17 stands out due to an intermediate creep phase and stress cycling, thus this core will not be considered in this context.

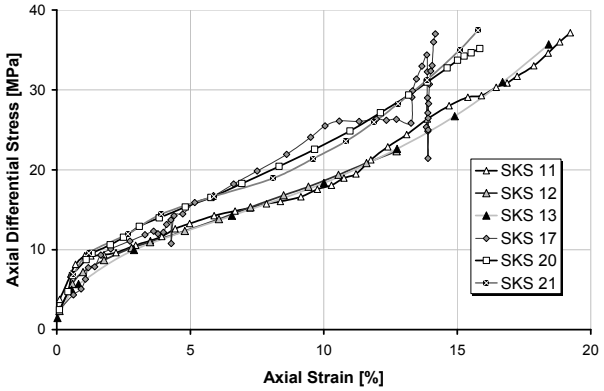

Fig. 4.4. Axial differential stress versus axial strain for Stevns Klint cores depleted close to reservoir conditions. Note: SKS 17 experienced creep and load cycling from 10% axial strain.

The five remaining cores gather in two groups as seen in Fig. 4.4; SKS 11, 12 and 13 in Fig. 4.5(a), deform similarly and significantly more than SKS 20 and 21 in Fig. 4.5(b). However, the cores in Fig. 4.5(a) are loaded with significantly different load rates, SKS 11 and 13 are depleted at 31 MPa/day and SKS 12 is depleted at 1 MPa/day. Similarly in Fig. 4.5(b); SKS 21 is depleted at 31 MPa/day, and SKS 20 at 1 MPa/day. Aside from minor experimental aspects, which are addressed in detail in paper III, the stress-strain curves lie almost perfectly on top of each other.

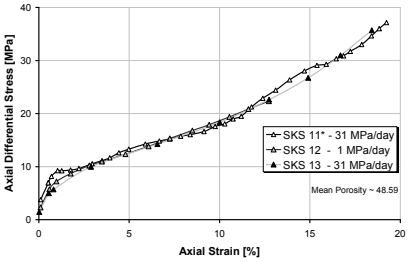

Fig. 4.5(a). Axial differential stress versus axial strain during depletion of SKS 11, 12 and 13. *alternating load rate.

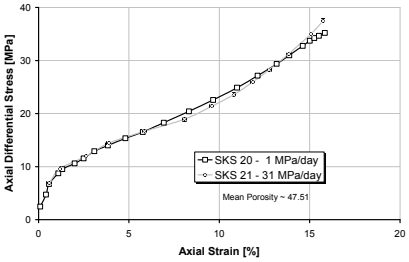

Fig. 4.5(b). Axial differential stress versus axial strain during depletion of SKS 20 and 21

In summary, these results suggest that the initial porosity rather than load rate determines the deformation behavior of the chalk, since the cores are simply categorized by initial porosity, in Figs. 4.5(a) and (b) with average porosity of 48.59% and 47.51%, respectively. In addition, knowing that SKS 17 had an initial porosity of 46.50%, the curves in Fig. 4.4 are roughly sorted by initial porosity as the group in Fig. 4.5(a) obtains more deformation than the group in Fig. 4.5(b), while SKS 17, accumulates the least deformation.

4.2.3 Fluid Drainage during Deformation

Even when the load rate is lowered from 31 to 1 MPa/day, cores with similar initial porosities deform similarly. Does this indicate that the load rate is not a governing variable for the deformation behavior? Fjær et al. (2008) state that low permeability materials like chalks need to be loaded sufficiently slow to obtain drained conditions. This implies that the degree of drainage might influence the deformation, causing rate dependent behavior. Jones (2002) suggested that local pore pressure increments, also called pressure lags (de Waal, 1986), may influence the degree of drainage and cause low permeable materials to achieve only partially drained conditions, even though the global pore pressure is kept drained. The apparent conflict between section 4.2.1 and 4.2.2, that rate dependent effects were observed when increasing the rate from 0.02 MPa/min (31 MPa/day) towards 0.06 and 0.08 MPa/min yet not when the rate was drastically decreased, might suggest that the cores were not sufficiently drained when the rate was increased towards 0.08 MPa/min?

Paper IV presents details from the pressure development for SKS 17, the same core as SKS 17 in Figs. 4.4. This core was tested close to reservoir conditions, however with a different boundary condition than for the other cores in Fig. 4.4. Instead of constant stress rate depletion, the pore fluid was produced at a fixed volume rate. A depletion program like this is more resembling to realistic reservoir depletion. The depletion phase was conducted in two stages for SKS 17, first by producing the pore fluid at a constant rate of 0.01 ml/min from 40 to 20 MPa. Then follows a 5 days long creep period, explaining the creep in Fig. 4.4, before depletion from 20 to 9 MPa. As illustrated in paper IV, the trend of the depletion is highly fluctuating, especially during pore collapse. Further, during the second depletion stage, the core experienced a pore pressure increase in terms of several MPa.

The irregular depletion of SKS 17 illustrates the importance of drained conditions. The load rate effects seen in section 4.2.1 and 4.2.2 have thus been discussed as effects of drainage constraints in the form of consolidation effects. For low permeable shale, Fjær et al. (1992) proposed a relation based upon Darcy's law (eq. 1.6), stating the degree of consolidation U to be a function of dimensionless time T_D, according to eq. 4.1:

$$U = U(T_D) \tag{4.1}$$

where T_D is given by eq. 4.2:

$$T_D = \frac{k\,t}{\mu\,C_m\,h^2} \tag{4.2}$$

T_D in eq. 4.2 is given by the permeability k, the viscosity of the pore fluid μ, the uniaxial strain compressibility C_m and the time t needed to equalize the pore pressure. Fjær et al. (1992) further state that T_D equals 2 at equilibrium pressure (U – *99.42%*). Equilibrium pressure is reached when the pressure gradient in the porous material, which was imposed by the applied load, has dissipated.

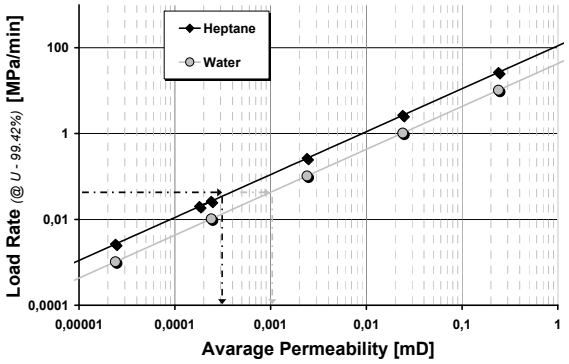

Fig. 4.6. Load rate versus average permeability at equilibrium pressure. Equilibrium pressure means approximately full degree of consolidation (U – 99.42%). The black curve represents a core saturated with heptane, the gray a core saturated with water.

The two curves in Fig. 4.6 are predicted using a C_m based upon Fig. 4.4, where the most extreme case indicates roughly 20% uniaxial strain at 40 MPa axial differential stress. Values of the load rate (40 MPa divided by t) are plotted versus k for two different scenarios; water and heptane, both at ambient conditions. The core is defined to have a length of 37.5 mm, yet only drained from one end. Accordingly, Fig. 4.6 shows that the average permeability may be as low as around 0.0003 mD (0.3 nanoD) when saturated with heptane and the core is not exposed to consolidation effects. The observations from Fig. 4.6 suggest that the load rate effects reported in section 4.2.1, yet not observed in section 4.2.2, may not be explained by consolidation effects.

4.2.4 Nucleus-of-Failure

Similar observations as for SKS 17 were further made and reported in paper IV: Additional cores were depleted following an isotropic stress path. These

cores were brought to their initial condition; a total isotropic stress of 27 MPa and a pore pressure of 25 MPa. The pore fluid was then produced, at fixed rates ranging from 0.01 to 0.1 ml/min; i.e. similar as for SKS 17. Then the pore pressure was shut in at certain levels during depletion while the response, both with respect to deformation and pore pressure, was monitored.

These isotropic depletion tests show that the pore pressure increased in all stages of loading. The response was minor in the elastic phase. However, as loading was continued further into the plastic regime, the response increased significantly, thus a stress state dependency was demonstrated. The average permeability needs to be drastically alternated if these observations are to be explained as consolidation effects, according to Fig. 4.6. However, studies have shown that the permeability does not change significantly during loading and deformation due to pore collapse of chalk (Christensen et al., 1992; Christensen, 1996). The stress state dependency thus suggests that the nature of the chalk failure and pore collapse, in advantage of the consolidation effects (e.g. Jones, 2002; Fjær et al., 2008), may describe the stress state dependency of the pore pressure increments in paper IV.

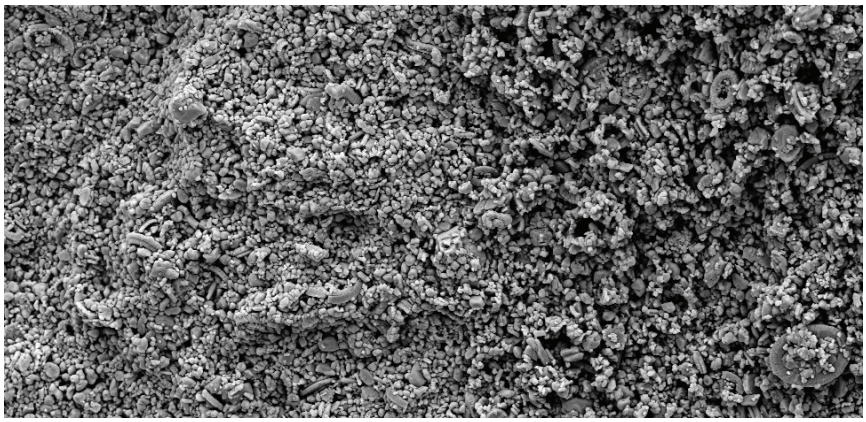

Fig. 4.7. SEM imaging after depletion and creep including SSW injection for core SKS 17, magnified 2.55K time

Andersen (1995) proposed the conceptual nucleus-of-failure model, introduced in section 1.4.1, describing the failure of the chalk including a rate dependent term. This concept may contribute to a better understanding of the apparent inconsistency between section 4.2.1 and section 4.2.2, as well as the irregular depletion of SKS 17 in paper IV. Sample SKS 17 was dismantled and prepared for further investigation by the use of a scanning electron microscope (SEM). The result of this SEM study is presented in Fig. 4.7. In addition to the depletion and early creep presented in paper III, SKS 17

experienced long term creep including injection of SSW as reported in paper VI. From this, it is fair to assume a strongly compacted homogeneous matrix structure (Powell and Lovell, 1994). However, the SEM-image in Fig. 4.7 reveals a non-uniform grain structure. The matrix to the left seems highly compacted while to the right more porous structure or less compacted zone is observed. This image is in contrast to the perception that plastic loading (>20% strain) induces fluid-like viscous behavior of the matrix. Contrary, these observations support the nucleus-of-failure concept, which suggest that different areas in bulk fail independently and load is transferred to stronger structures, thus preserving areas of higher porosity as observed in Fig. 4.7.

Smits et al. (1988), Ruddy et al. (1989), and Andersen et al. (1992a) all presents chalk compression studies performed under deformation controlled conditions, i.e., constant strain rate. This is a different boundary condition compared than the stress rate approach applied in this work and may therefore not be directly compared. The challenge when loading at constant strain rates is that the material may deform faster than the desired rate, especially during pore collapse, so-called softening. On the other hand, as shown in this work, the challenge is to load slow enough to allow the material to deform and thus avoid that the material shows a higher strength than it really possesses, according to the nucleus-of-failure concept (Andersen, 1995).

A possible explanation for the non-appearance of load rate effects in section 4.2.2, could be that the load rate of 0.02 MPa/min is sufficient slow to avoid accumulation of "delayed deformation." In a field scenario, with thick formations layers with low permeability and limited drainage, the effect of consolidation may not be disregarded. However, for this work it seems evident that the nucleus-of-failure, in favor of pore pressure gradients due to consolidation, provides a better understanding for the load rate observations in paper III.

4.2.5 Creep Mechanisms

As reported in paper III, the transient creep seems to be strongly related to the load rate. Fig. 4.8 shows the normalized axial creep versus creep time for the cores SKS 11, 13, 17 and 20, where transient creep separates the curves from the very beginning. SKS 11 and 13 were depleted at 31 MPa/day, while SKS 20 was depleted at 1 MPa/day. As mentioned in section 4.2.3, SKS 17 spent about 5 times longer in depletion than SKS 11 and 13. It therefore lies between samples SKS 20 and SKS 11 and 13. Since load rate seems to affect transient creep it may be argued that the mechanism of transient creep is

explained by nucleus-of-failure, not by consolidation, as all curves in Fig. 4.8 are loaded slow enough to ensure fully drained conditions (Fig. 4.6).

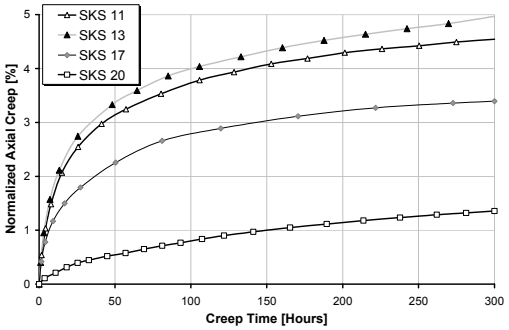

Fig. 4.8. Axial creep strain versus 300 hours of creep for the SKS 11, 13, 17 and 20.

When investigating the creep rate, Fig. 4.9(a), it is shown that all samples show similar creep rate after about 175 hours of creep. According to paper III and Fig. 4.9(a), this observation also applies for K 14 and R 26, which fit well with the four Stevns Klint cores from Fig. 4.8. This may suggest that the effect of the load rate during the depletion period is lost after 175 hours of creep. From the nucleus-of-failure concept, this may be understood as if the cascade of failure has diminished after 175 hours.

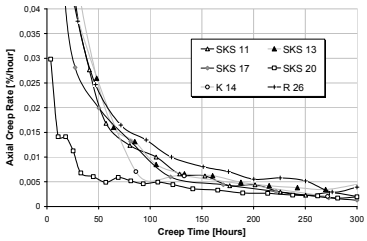

Figure 4.9(a) Creep rate versus 300 hours of creep for SKS 11, 13, 17, 20, K 14 and R 26.

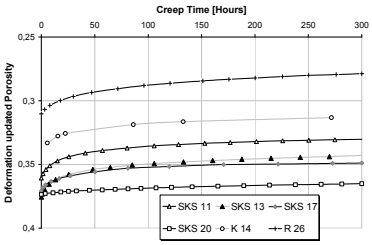

Figure 4.9(b) Porosity development versus 300 hours of creep for SKS 11, 13, 17, 20, K 14 and R 26

Given that the creep after 175 hours is solely steady state, it may be proposed that steady state creep seems to be independent of most other variables, since cores from the two outcrops (Stevns Klint and Kansas) and the reservoir core creep similarly. It is possible that this is the true creep that is captured, which is independent of the load rate. This universal creep rate may be dependent on properties the samples have in common such as stress level, pore fluid saturation and temperature. Ultimately, the most important property is most likely the mineralogy; it seems like the intergranular friction governs the universal creep mechanism.

4.2.6 Porosity Influence on Creep

The deformation behavior of chalk has often been described as a function of initial porosity (e.g. Engstrøm, 1992; Havmøller and Foged, 1996b). If porosity development versus creep time is plotted, as in Fig. 4.9(b), it may be seen that all cores creep similarly. The starting point for the curves is the post-depletion porosity. These curves do not seem to move towards a common porosity, but exhibit parallel behavior to each other. From this, it may be suggested that deformation due to increase load and due to creep are independent processes: The deformation obtained due to depletion seems to be strongly influenced by porosity, while steady state creep is not (Figs. 4.9(a) and (b)).

If this suggestion is valid, the contribution of steady state creep should be an independent element in a total accumulated strain equation. Transient creep, whether due to local pressure lags, pore pressure gradients or the nature of chalk failure explained by the nucleus-of-failure concept, is however strongly dependent on the load rate. It should be mentioned that these suggestions are based on rather few tests, and although they had a large variation in initial porosity, the post-depletion porosity, i.e. the porosity prior to creep, only varies from 0.31-0.38 in Fig. 4.9(b). To strengthen the suggested hypothesis, a greater range of porosities should be investigated.

4.3 Hardening of the Chalk

The plastic deformation in the high porous chalk, either due to increased load, creep or potentially water weakening, results in enhanced strength. Paper III demonstrates the importance of real-time moduli values and relates this increased stiffness directly to the decrease in porosity, which is covered in section 4.3.1. Chalk hardening in a *q-p'* context using an example from paper VI is discussed in section 4.3.2.

4.3.1 Updated Plastic Uniaxial Strain Modulus

Fig. 4.10 presents the axial differential stress plotted versus axial strain for SKS 11, 13, 20 and 21, and K 14, 18 and 19 from paper III. The difference in strength between the high porosity Stevns Klint and medium porosity Kansas cores is obvious. The Kansas cores deform roughly one fourth compared to the Stevns Klint cores. The average of the uniaxial strain moduli found from

the linear slope of the plastic curve, are reported to equal 0.12 and 0.42 GPa for the Stevns Klint and Kansas cores, respectively, (paper III).

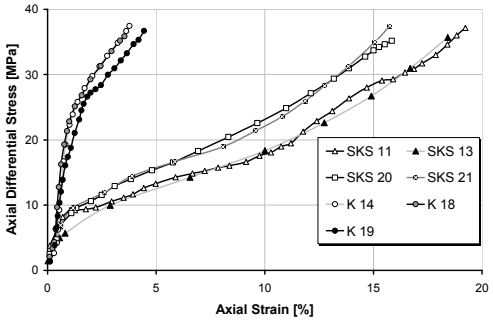

Fig. 4.10. Axial differential stress versus axial strain for SKS 11, 13, 20 and 21, K 14, 18 and 19. Note that the Stevns Klint cores experience significant nonlinear hardening.

The Stevns Klint cores in Fig. 4.10 do all experienced pronounced nonlinear hardening. The curves are bending upwards towards the end of the loading. One value of the plastic uniaxial strain modulus does not capture such nonlinear behavior. Paper III suggests an alternative method for determining the uniaxial strain modulus, calculating ratios along the plastic curve using smaller strain steps, i.e. the derivative of the curve. Such modulus values are plotted versus accumulated plastic strain in Fig. 4.11(a). The Kansas cores experienced a gradual yielding which explains why the Kansas modulus curves decrease from around 1.4 towards 0.45 GPa before stabilizing. There is a clear difference in stiffness as the three Kansas cores obtain three times the stiffness of the Stevns Klint cores; roughly 0.45 GPa compared to 0.15 GPa after 3% accumulated plastic strain. The Stevns Klint cores accumulated around 4 times the plastic strain of the Kansas cores, and moreover, showed distinct increase in stiffness as they deformed corresponding to the distinct nonlinear hardening observed.

It is a fairly well established protocol to link the measured plastic modulus to the initial porosity of the core. However, for high porosity material like the Stevns Klint samples in Fig. 4.10, the porosity is dramatically changed during the process of determining the modulus. Obviously, this is more relevant for plastic than elastic values, since the deformation obtained during elastic loading does not usually alternate the porosity significantly: SKS 13 experienced a porosity drop during elastic loading of 0.3%, but dropped in total from 49.0% to 37.5% during the depletion in Fig. 4.10 (it dropped additionally to 33.3% due to long term creep and water weakening, paper VI). As a reply, paper III introduces a plastic uniaxial strain modulus as a function of real time porosity, updated according to accumulated strain. The advantage

using this alternative technique for presenting the plastic modulus is two-sided. Firstly, it accounts for non-linear hardening. Secondly, it predicts a more accurate plastic modulus for in-situ rock formations as it accounts for the porosity alternation during the measuring process.

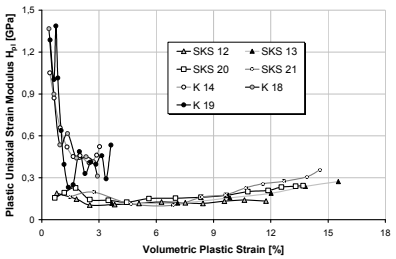

Fig. 4.11(a). Plastic uniaxial strain modulus versus normalized plastic strain for Stevns Klint and Kansas samples.

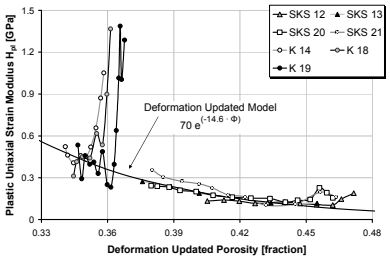

Fig. 4.11(b). Uniaxial plastic strain modulus versus deformation updated porosity for Stevns Klint and Kansas samples.

The modulus values from Fig. 4.11(a) are plotted versus updated porosity in Fig 4.11(b). The data for both the Kansas and Stevns Klint cores generally fit the same trend given by eq. 4.3;

$$H_{live} = 70 \cdot e^{-14.6 \cdot \phi} \qquad (4.3)$$

where H_{live} is the plastic uniaxial strain modulus, and ϕ is the porosity calculated for the measured strain. In literature, it is common to present moduli values as dependent on stress (e.g. Zisman, 1933; Janbu, 1985), but also possibly to present stiffness of porous media as dependent on porosity, as Skempton (1961) did from a theoretical perspective. The fit in Fig. 4.11(b) is a significant observation in the way that hardening is described by the decrease in porosity, and that the Stevns Klint and Kansas cores seem to fit the same trend. Finally, a greater porosity span including chalk from other locations should preferentially be tested before this fit could be generally accepted.

4.3.2 Hardening in a 2-Dimensional q-p' Diagram

The 2-dimensional *q-p'* diagram introduced in section 1.3 and reviewed in paper VI may be used to illustrate hardening of chalk. Assuming that hardening is a reflection of the decrease in porosity (Teufel and Rhett, 1991), hardening may be illustrated in a *q-p'* diagram as multiple yield surfaces, each with its own porosity. Such porosity dependence is equivalent to the void ratio dependence, where void ratio is the third dimension in a three dimensional

yield space proposed for clay behavior (e.g. Atkinson and Bransby, 1978, Fjær et al., 2008). Indeed, Jones (1994) showed that chalk loaded at uniaxial strain conditions may be described by such a three-dimensional yield space in the two-dimensional *q-p'* diagram extended with porosity or void ratio as the third dimension.

Paper VI describes hardening as updating of the 2-dimensional yield surface. As the core compacts, the end-cap will expand according to its new porosity. The initial shear failure line, which makes up the border towards shear failure, will after failure not be defined, as the chalk loses its cohesion (Risnes et al., 1994; 1998). Now the critical state line makes up the border towards the impossible states. Finally, it is assumed that water weakening also updates the yield surface (Risnes et al., 2001; Madland et al., 2002; Risnes et al., 2003), and porosity and water weakening are assumed as independent processes both affecting the strength of the chalk. The physical meaning of an end-cap dependent on porosity, instead of maximum stress, is significant: The porosity reduction due to creep may now expand the end-cap, even though the stress state remains the same. Paper VI emphasizes on core SKS 11 to illustrate such hardening in a *q-p'* diagram.

4.3.2.1 SKS 11 as an Example

The depletion and early creep for core SKS 11 from Fig. 4.4 is presented in detail in paper III whereas the long term creep and water weakening are covered in paper VI. The focus in this section is two incidental load cycles that took place during the creep phase, which caused additional plastic compaction as described in paper VI. Since the stress increments are unloaded and at the same time the strains were plastic, such compaction would result in a drop in porosity, while the stress state is equal to the conditions before the incidental load cycles. The entire test history of SKS 11 is presented in Fig. 4.12(a), where the creep starts from around 19% axial strain and 37.5 MPa axial differential stress. The two stress increments can be seen as two peaks in the figure, the first increment roughly 6 MPa, the second around 8 MPa. As reported in paper VI, the creep basically stops after the two stress cycles, even during injection of synthetic seawater, SSW.

The stop in creep experienced for SKS 11 was in Paper VI explained by the hardening process, causing the yield surface to expand. Fig 4.12(b) summarizes the end-cap evolution according to the stress versus strain history in Fig 4.12(a). The gray yield surface in the illustration (Fig. 4.12(b) is the imaginary initial yield surface prior to yield. Then the core was loaded from the initial stress state (the circle inside the gray envelope) towards the

depleted stress state, located on the new updated black end-cap. Since the material has now failed in pore collapse, the critical state line *CSL* represents the upper limit towards shear failure.

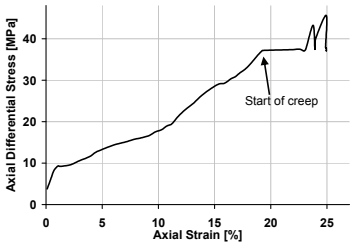

Fig. 4.12(a). Axial differential stress versus axial strain for SKS 11.

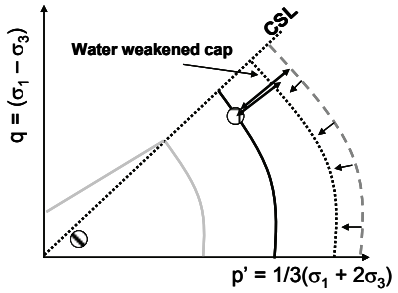

Fig. 4.12(b). Axial differential stress versus axial strain for SKS 11.

As mentioned, the black end-cap represents the core. As described in detail in paper VI, due to transient creep and the two stress cycles, the end-cap is further expanded, causing the depleted stress state to be positioned well inside the new, now gray stippled end-cap. The suggested explanation for why the creep basically stops is represented by the black dotted end-cap in Fig. 4.12(b). According to previous research (Risnes, 2001; Madland et al., 2002; Risnes et al., 2003), the end-cap is expected to shrink due to water weakening. Such water weakening is illustrated in Fig. 4.12(b) by the arrows showing that the end-cap now shrinks to the black dotted end-cap. However, the end-cap obviously did not shrink enough as no water weakening impact on the creep rate was observed. Paper VI suggests that this may be due to the two mentioned stress cycles; the end-cap was simply pushed too far, making the water weakening too small for additional deformation.

4.3.2.2 Effect of Hardening on Water Weakening

Madland et al. (2002) showed that the yield surface of chalk is strongly dependent on the pore fluid. Specific values of hydrostatic yield for tests on both oil and water saturated Maastrichtian outcrop chalk may be found in that study. These values changed from 17 to 10 MPa as a function of pore fluid. 17 MPa is representing oil saturated chalk and 10 MPa is representing water saturated chalk. Havmøller and Foged (1996b) proposed a relation between hydrostatic yield stress and porosity for Maastrichtian chalk. The relationship indicates the porosity to be 45.1% and 40.5% for chalk that yields at 10 and 17 MPa hydrostatic yield, respectively. Given that the yield surface of chalk is a function of both porosity and fluid saturation, both being independent of each other, it may be suggested that the development of the end-cap due to water injection corresponds to a porosity decrease in the range of 4-5%.

Indeed, the porosity drop due to creep for SKS 11, including the two incidental load cycles gives in total a porosity drop of around 4.3%, exceeding its current stress state. Thus may be a possible explanation behind the lower additional strain observed when injecting SSW.

In addition it is interesting to notice that cores experience creep even though they are located well inside the so called end-cap or yield surface. This was also reported by Risnes and Nygaard (1999). SKS 11 clearly pushed the end-cap (decreased the porosity) due to the two stress cycles shown in Fig. 4.12(a), however, there is still some minor creep, as reported in paper VI. This suggest that steady state creep and deformation due to change in stress are different and independent physical processes, which is also seen in subchapter 4.2.

4.4 Stress Path Observations

The stress path for testing at uniaxial strain conditions in a *q-p'* context is discussed in this sub-chapter. The findings reviewed mainly originate from the high porosity Stevns Klint cores in paper III, as these cores showed the most distinct plastic behavior as well as the span in load rate (1 – 31 MPa/day).

4.4.1 Time Dependent K_0 Behavior

The stress path results in paper III confirm previous results of the K_0 stress path. Fig. 4.13 is an illustration attempting to capture the observed and confirmed chalk behavior. As shown by Leddra et al. (1990), Loe et al. (1992) and Jones et al. (1994), the K_0 stress path obtained a rather low value, around 0.3 prior to yield, a transition period with a stress path around unity and finally a stable path during plastic phase around 0.6. Fig. 4.13 illustrates this, with a steep path from *A* to *B* and then a horizontal transition during pore collapse from *B* to *C*.

The new observation in paper III is that a time dependency of the stress path was observed. Fig 4.13 shows this in a schematic way, where rapid loading results in a rather long transition period in terms of stress units, as the curve entered the stable plastic trend at C_{fast}. The results indicate that this transition period is not only shorter, but also that the slope of the plastic path gets steeper as the rate is lowered, marked as C_{slow} and D_{slow}. Moreover, when the

samples that were loaded rapidly were left to creep at uniaxial strain conditions, the horizontal stress had to be increased to maintain no lateral movement, thus a change in stress state similar to the movement from D_{fast} to E_{creep} was observed.

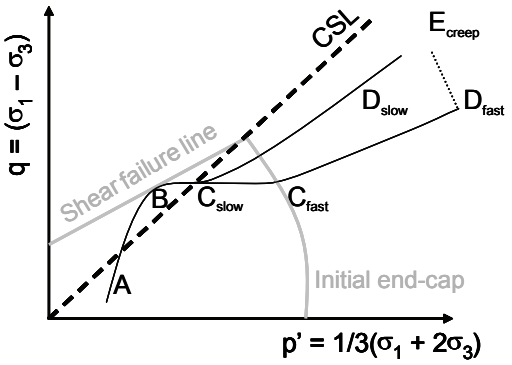

Figure 4.13. Sketch of the yield envelope including the critical state line *CSL* and two K_0 paths; slow and fast.

The discussion in paper III stated that such time dependency was probably not due to consolidation or related to drainage. This discussion is further strengthened by the arguments in section 4.2.3; the load rate is far lower than the lower limit for obeying drained conditions. The nucleus-of-failure concept (Andersen, 1995) may be directly related to what paper III describes as time dependent hardening of the chalk. Gutierrez et al. (1992) also showed that the pore collapse mechanism of chalk seems to be a gradual process. This is also discussed in paper IV and observed from the SEM-image in Fig. 4.7 as some parts of the chalk seem less compacted than other areas.

As discussed in section 4.2.4, load may be applied faster than the material is able to deform due to the phenomenon described by the nucleus-of-failure concept. This would lead to chaos and build up of local stresses, and the grains will slide dramatically. Such grain sliding or re-organization of the matrix structure after pore collapse seems to be a time consuming process. From this it may be suggested that the time dependency of the stress path is explained by the nucleus-of-failure concept. Paper III reports values of K_0 during elastic loading to be roughly in the range of 0.25-0.35, only R 26 stands out with even lower K_0. However, when the cores yield and experience plastic deformation, the stress path K_0 is close to 1. As this stage of pore collapse is characterized by chaos contrary from the more stable elastic stage, the value of K_0 may be regarded as an indirect measure of the stability of the grain structure: A higher value represent less stability or rigidity. From this definition of K_0, it is interesting to observe that there is a significant spread in

K_0 for the cores in their plastic stages. All cores loaded at a strain rate of ≥0.02 MPa/min, obtained a K_0 of 0.49-0.60 in the stable plastic stage, R 26 included, as reported in paper III. However, the slowly loaded cores, SKS 12 and 20 obtained significantly lower K_0 values; 0.45 and 0.46 respectively. It may be proposed that the more slowly the core is loaded, the more stability it acquires in the actual loading which is indirectly reflected in a lower value of K_0.

4.4.2 Critical State Considerations

The combined trend of the time dependency demonstrated in paper III and illustrated in Fig. 4.13 suggests that the uniaxial strain stress path approaches the critical state line *CSL*. The critical state of a material is the point where compactional and dilatant behavior coincides. The critical state line is found when critical points are plotted for different porosities of the same material in combination with porosity dependence in the 2-dimensional *q-p'* plot described in detail in section 4.3.2. This line represents an ultimate state where large shear strains may occur with no change in shear stress for plastic loading (Fjær et al., 2008).

The definition of the uniaxial strain is basically a boundary condition that prevents a sample from globally failing in shear, since the activation of such failure would result in global shear strains, i.e. expanding radial movement. Thus when shear failures start to develop, the horizontal stress is increased in order to prevent such radial movement. Too much horizontal stress induces compactional radial movement, which is also a violation of the boundary condition. The stress path during uniaxial strain testing is thus really a balancing contest between the two types of radial movement.

The time dependency of K_0 indicates that the path in the plastic region is moving closer to the *CSL*. The transition phase where the stress path is close to unity, from *B* to C_{slow} or C_{fast} in Fig. 4.13 may be explained by the cohesion of the material. The shear strength in intact chalk allows it to be localized to the left of the CSL, until it fails and loose the cohesion. In this moment, when the sample starts to fail and goes from an elastic to a plastic material, it needs to transfer away from the state that promotes dilatant behavior. The time dependency also suggests that this transition stage gets smaller, which may be explained by the nucleus-of-failure concept as well. When a material is loaded slower, more of the deformation will have occurred before new load is applied, thus the core will be localized closer to the *CSL* when entering the stable plastic path.

5 Simulation of Reservoir Processes

5.1 Water weakening close to reservoir conditions

The two first sections focus on effects of chemical mechanisms caused mainly by magnesium, both at low and high pore pressure and the analysis shows evidence of mineral precipitation. The following sections investigate the effect of SSW injection on cores subjected to long term creep close to reservoir conditions

5.1.1 Rate Dependent Effects of Magnesium

Several studies investigating chemical water weakening (Heggheim et al., 2005; Madland et al., 2006; Korsnes et al., 2006a; Korsnes et al 2006b; Korsnes et al., 2008a; Madland et al., 2008; Zangiabadi et al., 2009; Madland et al., 2009) have, as introduced in section 1.5, identified two main mechanisms responsible for the weakening of chalk by seawater-like brines. These are the substitution of calcium by magnesium in the presence of sulfate hypothesis, and the precipitation of mineral(s) that trigger(s) an enhanced dissolution of calcite. In order to gain further insight into the complexity of this matter, chalk cores were mechanically tested; saturated and flooded with simpler brines to isolate the effect of the individual ions.

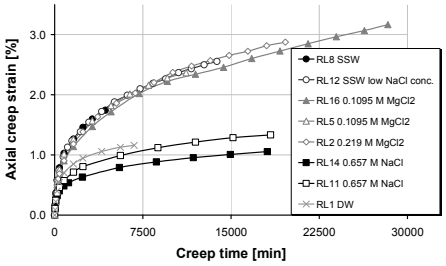

Fig. 5.1(a). Axial creep versus time for Liege cores flooded with DW, $Na_{0.657}$, $Mg_{0.109}$, $Mg_{0.218}$ and SSW brines

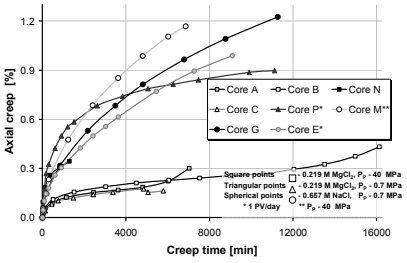

Fig. 5.1(b). Axial creep versus time for Stevns Klint cores flooded with $Na_{0.657}$ and $Mg_{0.218}$ at high and low pore pressure

The mechanical results in paper V indicate that magnesium chloride brines have a huge impact on chalk strength, demonstrated clearly in the creep phase. Fig. 5.1(a) shows creep for Liege cores. Cores flooded with magnesium

chloride brines obtain similar creep as cores flooded with seawater-like brines. Further, both these brines obtain far more deformation than cores flooded with sodium chloride brines or distilled water. The opposite is seen for the Stevns Klint cores in Fig. 5.1(b). The cores flooded with magnesium chloride show less creep, and more importantly, the steady state creep rate is significantly lower than the three cores flooded with sodium chloride. In addition to this contrast, all cores flooded with sodium chloride brine, regardless of chalk type, deform rather similarly. After 10.000 minutes, the two Liege cores showed 1.0±0.1% creep, and the three Stevns Klint cores, if all had experienced 10.000 minutes of creep, would be localized roughly at 1.1±0.1% creep.

Paper V put focus on the creep rate in the steady state creep phase as an indicator of the ongoing weakening. There is obviously a difference between the Stevns Klint material and the Liege material when it comes to effects of the magnesium chloride brine. However, a rate effect for Stevns Klint chalk by core A and B in Fig. 5.1(b) is seen. These were flooded with magnesium chloride and tested at high pore pressure (40 MPa). They are distinct as the deformation accelerated after approximately 3 (core A) and 8 (core B) days of creep. Paper V reports that the creep rate was increased by a factor of more than 12. The two cores failed shortly after this increase was initiated, thus the phenomenon should be further studied. However, it is suggested that a rate effect exists when magnesium is interacting with Stevns Klint chalk. And further, the reason for the accelerating creep observed in core A and B may be a delayed effect, advanced and promoted by the high pore pressure.

5.1.2. Evidence of Precipitation and Dissolution

Despite the difference in mechanical behavior when flooding magnesium chloride brine, chemical analysis of the sampled effluent suggests that similar chemical reactions are taking place. A significant amount of magnesium was lost in the core while at the same time considerable amounts of calcium were produced. Chloride seems to be more or less inert to the chalk surface. Close investigation of the data showed that the Liege cores loose more magnesium and subsequently produced more calcium than for the Stevns Klint cores tested at low pore pressure. However, the Stevns Klint cores tested at high pore pressure produced slightly more calcium than those at low pore pressure.

Nevertheless, similar chemical reactions are taking place, and calculations presented in paper V point out that the calcium produced exceeded the limit of what could be predicted by the substitution theory. Further, these

considerations suggest that the mechanism for the mechanical response is precipitation of a mineral according to the introduction in section 1.5.2. The predicted precipitation of new minerals was indeed verified by SEM. Even though the exact nature of the precipitates formed remains undetermined, paper V suggests that at least two types of magnesium-bearing minerals are formed. These are both shown in Fig. 5.2. Firstly, one or more magnesium bearing carbonate minerals is shown in the left picture (a) in Fig. 5.2, where the calcite grains are covered by tiny minerals.

Paper V further reports that such minerals, possibly huntite $CaMg_3(CO_3)_4$ and magnesite $MgCO_3$ are likely to precipitate in Stevns Klint chalk when flooding magnesium chloride brines at 130 °C. Secondly, the right picture (b) in Fig. 5.2 displays another type of mineral, characterized as a possible silicate mineral with a clay-like appearance in addition to magnesium. For such a mineral to precipitate, it consequently requires that silicates originally present in chalk need to be dissolved and re-precipitated together with magnesium. These minerals are seen as coatings on the grains, almost like a web covering the calcite grains. This is limited to chalks containing sufficient amount of non-carbonate content, in this case Liege chalk.

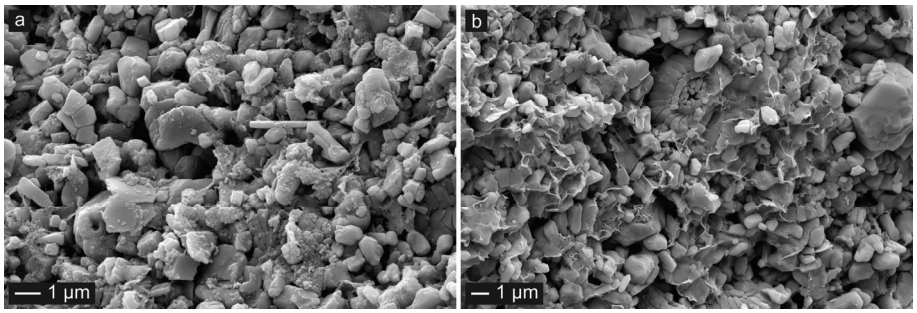

Fig. 5.2. SEM image of Liege chalk flooded with $Mg_{0.1095}$. Evidence of newly precipitated magnesium-bearing minerals. (a) display calcite grains covered with aggregates of tiny (carbonate?) minerals. (b) show calcite grains covered with clay-like (silicate?) minerals.

The clay-like precipitates in Fig. 5.2 are less likely for Stevns Klint chalk, since this chalk is cleaner than Liege chalk. Some of the explanation for the difference in strain observed in Figs. 5.1(a) and (b) may thus be hidden in the nature of the mineral(s) precipitated. Obviously, the forming of new, rather dominant minerals as displayed in Fig. 5.2 could influence the intergranular friction, which may be the link between the chemical mechanism and the mechanical strength and stability of chalk.

5.1.3 Impact of Initial Brine Saturation

Schroeder et al. (1998) reported that the deformations induced by water-flooding occur in two steps; an instantaneous response, probably caused by physico-chemical effects (Risnes, 2001) and then a creep-like behavior after the chalk gets in contact with water. Korsnes et al. (2006a) demonstrated such behavior: A decane saturated core went from creeping ~0 %/hour to experience dramatic instantaneous strain (>2%) and a clear shift in the creep rate when flooded with water. Such dramatic response was not seen for the long term creep with SSW injection in Paper VI.

Studies have shown that only a small degree of water saturation is needed to mobilise the water weakening effect (Schroeder et al., 1998; Madland, 1999; Risnes, 2001; Risnes et al., 2005). These studies were performed at low temperature and a water/air system, a water/model-oil or a water/glycol system were investigated. The long term creep with SSW injection in Paper VI is performed at high temperature (92 °C), involving AVB, HP and SSW according to Table 3.1. The results are therefore not completely comparable to the previous studies.

However, it is proposed that the absence of any instantaneous dramatic water response could be related to the water saturation present in the cores. The initial brine saturation (~5-8%) was, as discussed in paper VI, probably alternated by the huge deformations during depletion and resulting compaction. By assuming that the initial brine saturation remained residual during depletion, it is fair to assume that the cores approached 10% brine saturation when the SSW was injected.

5.1.4 Volume Dependent SSW Effect

The observed weakening from paper IV is represented by Figs. 5.3. Fig. 5.3(a) shows the creep for SKS 17; a clear shift in the curve is seen as continuous injection of 3.29 pore volumes, PV, of SSW per day is initiated from 353 hours of creep. Paper VI reports that the creep rate in general doubles as SSW enters the cores, which is also the case for SKS 13, Fig. 5.3(b). However, the creep rate declines when the injection of SSW stops. This observation confirms that the SSW weakening in possibly already water weakened cores is caused by ongoing chemical processes depending on injected volume.

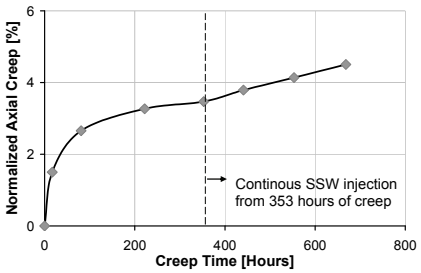

Fig. 5.3(a). Axial creep versus time for SKS 17, continuous flooding of 3.29 PV of SSW per day after 353 hours.

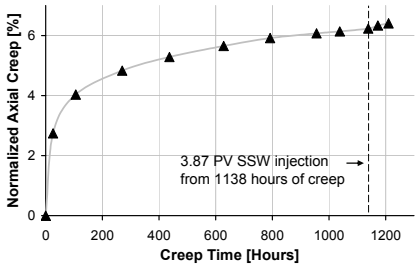

Fig. 5.3(b). Axial creep versus time for SKS 13, 3.87 PV of SSW injected after 1138 hours.

Studies reported that cores flooded with SSW experienced similar development of the magnesium and calcium concentration in the effluent as observed for the cores flooded with magnesium chloride brine in section 5.1.1 (Korsnes et al. 2008a; Madland et al. 2009). Paper V suggests that the chemical mechanism that takes place when flooding SSW is similar to flooding magnesium chloride brine, i.e. precipitation of (a) supersaturated mineral(s) that subsequently trigger dissolution of calcium.

In addition to the calcium and magnesium development, cores flooded with SSW also experienced a reduction in sulfate (Korsnes et al. 2008a; Madland et al. 2009), which points towards precipitation of anhydrite $CaSO_4$ inside the core (Hiorth et al. 2008), in addition to a magnesium-bearing mineral.

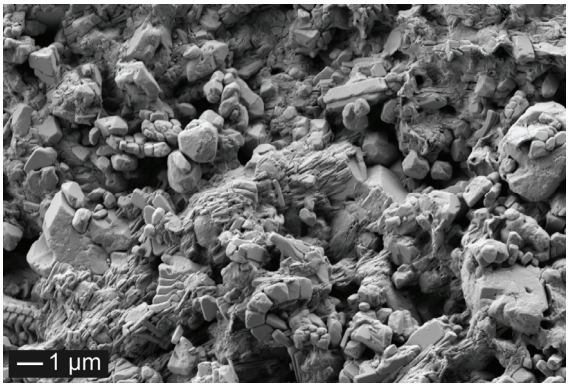

Fig. 5.4. SEM micrograph of a Liege core, paper V, after flooding with SSW with low NaCl concentration; aggregates of bladed-massive anhydrite precipitates partly fill the pore space.

This assumption is further strengthened by the observation indicating that the calcium produced does not completely match the magnesium lost for the cores flooded with SSW, and that paper V shows precipitation of anhydrite in a Liege core flooded with SSW with low sodium chloride concentration. This

differs from the cores flooded with magnesium chloride brines, where results presented in paper V indicate that the loss in magnesium is matched by the produced calcium. The anhydrite precipitation is seen in Fig. 5.4, which displays anhydrite acting like pore filling cement. The tests in paper V are performed at 130 °C, whereas the experiments in paper VI are performed at 92 °C. However, it is likely that a reduction in sulfate concentration occurs at 92 °C as well, similar to results by Korsnes et al. (2008a).

Even though the cores in paper VI show a rather modest effect of SSW injection, they are in contrast with the results of Rhett (1990), who found that seawater had negligible effect on short and long-term compaction behavior for chalk already wetted with an aqueous phase. Further, Rhett (1990) suggested that the dominant mechanism for water weakening is likely adsorption of water on solid calcium carbonate surface. The chemical weakening studied in paper VI occurred in already water wet cores and the effect is enhanced by more injection, thus adsorption of water does not seem significant for these cores.

5.1.5 Creep Prediction

As mentioned in section 1.4.2, Andersen (1995) named two main models for predicting time dependent behavior or creep that have been applicable for chalk. They are the de Waal model (de Waal, 1986) and the inverse plotting method introduced by Johnson et al. (1989). Paper III showed that the de Waal model overestimated the creep for the Stevns Klint cores, while underestimating the curves for the Kansas material. The inverse plotting method on the other hand does not actually produce a linear trend as it was intended to do (Andersen et al., 1992b). Nevertheless, the inverse plotting method is utilized in this section, similar as in paper VI, to provide approximate values for expected creep as close as possible to infinite time.

Fig. 5.5(a), (b), (c) and (d) shows the inverse of creep for SKS 17 and 13, K 14 and R 26 plotted versus the inverse of time. As reported in paper VI, SKS 17 in Fig. 5.5(a) was exposed to continuous injection of synthetic seawater, SSW, which permanently changed the creep rate. When plotting the creep data from paper VI according to the inverse plotting method a clear shift in the trend with SSW injection was observed. If the linear trends prior to and after SSW injection are extrapolated towards infinite time $t^{-1} = 0$, this simple prediction method suggests 3.86% creep without SSW injection and 6.94% creep with continuous injection of 3.29 pore volumes, PV, per day. The

relative effect of SSW is thus another 80% creep at infinite time compared to the extrapolated trend prior to SSW injection.

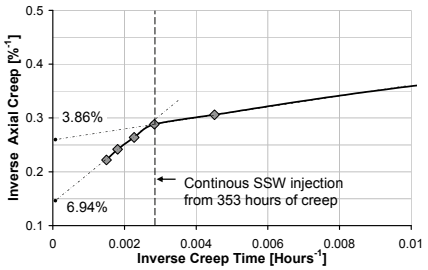

Fig. 5.5(a) Creep Prediction for SKS 17, continuous SSW injection (3.29 PV/day)

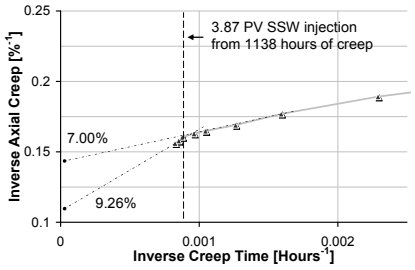

Fig. 5.5(b) Creep Prediction for SKS 13, 3.87 PV SSW injected

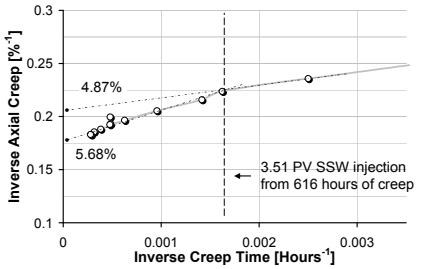

Fig. 5.5(c) Creep Prediction for K 14, 3.51 PV SSW injected

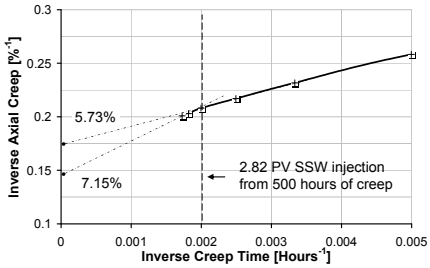

Fig. 5.5(d) Creep Prediction for R 26, 2.82 PV SSW injected

SKS 13, Fig. 5.3(b), experienced a less significant effect. This is explained by the limited volume of SSW injected (3.87 PV), section 5.1.4. The creep prediction for SKS 13, despite that the test failed shortly after SSW injection (see paper VI), estimates the effect of SSW to be 32% additional creep at infinite time compared to without any SSW injection, Fig. 5.5(b). Similarly, K 14 in Fig. 5.5(c) and R 26 in Fig. 5.5(d) showed 17% and 25% additional creep due to the SSW injection, respectively. The predictions does not account for the downwards bending as reported by Andersen et al. (1992b), and it is worth mentioning that such downwards bending was actually seen for some of the creep in paper VI, e.g. K 14, Fig. 5.5(c). However, these predictions are only intended to serve as rough indications of the influence of SSW, which is further used in section 6.2.2. The average data from Figs. 5.5 may be summarized as follows: 5.36% creep without any SSW (the average of the predicted ultimate stain from Figs. 5.5), extra 25% for ~3 PV (2.82 – 3.87) of SSW and finally 80% extra strain with continuous injection of 3.29 PV SSW per day.

5.2 Acid Stimulation

Wells in the North Sea chalk reservoirs are, according to the introduction in section 1.6, frequently treated by acid stimulation. The acid is intended to differential etch the walls in hydraulically induced fractures, however, the actual induced geometry is uncertain. The objective of paper VII has thus been to test existing theories by stimulating chalk samples. 47 stimulation experiments were performed which are presented in section 5.2.1 and 5.2.2.

5.2.1 Dependency of Rock Properties

Fig. 5.6 highlights the main observation from paper VII, as the figure shows the difference between a low porosity core, a medium porosity core and a high porosity core, marked with A, B and C, respectively.

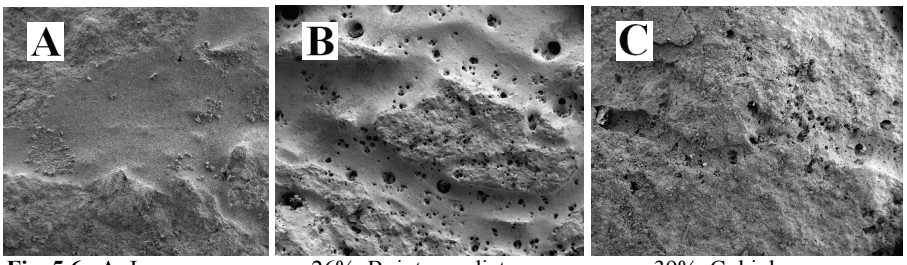

Fig. 5.6. A; Low porous core ~26%, B; intermediate porous core ~39%, C; high porous core ~47%. The SEM images are magnified 45 times

All three pictures are 45 times magnified SEM pictures taken from the fracture plane in which the acid was injected. The low porous Kansas material in SEM image A shows that the acid has created smooth areas in the fracture, like a channel. Image B represents the intermediate porosity Kansas material and also shows that smooth channels are created, yet with multiple leak-off holes into the matrix. The image representing the high porosity Aalborg chalk, C, shows that there is hardly any creation of a channel pattern, as all acid has leaked off into the matrix. This is significant, and suggests that acid stimulation in high porosity chalk is, regardless of the presence of a hydraulic fracture, achieved by acid propagating into the chalk as a matrix stimulation rather than acid fracturing stimulation.

5.2.2 Dependency of Stimulation Method

The dependency of the stimulation method used was in paper VI categorized in two groups; effects of the injection rate and flux and the effects of injected volume and concentration. If the acid was flooded slowly though the core the residence time for the acid to react with the matrix will increase. Core A and B in Fig. 5.7 are stimulated equally yet with different injection rate: The images show that the acid will dissolve chalk close to the injection site where a cavity is created for core A. Contrary only small holes are left at the injection site for core B, which was stimulated with higher rate. Observations show however, that a higher injection flux may actually cause more chalk to be dissolved close to the inlet, which may be related to more turbulent flow associated with higher rate.

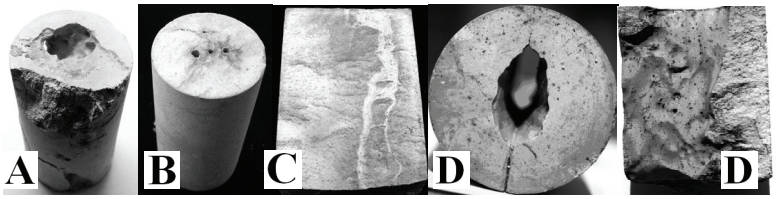

Fig. 5.7. Acid stimulated cores; A & B is Aalborg cores with low and high flooding rate, respectively. C – fracture flooding low porosity Kansas core. D high volume stimulation of an intermediate porosity Kansas core.

Dong et al. (1999) concluded that the areas on both sides of the created acid channel within the fracture will not be reached by the acid. Fig. 5.7 shows the opposite effect, with dark acid tracer marks covering the entire fracture face. After time, the acid selects the easiest pathway and creates a channel shown as the light area in Fig. 5.6(C). Common for all cores is that the more acid injected the more inlet etched. Core D in Fig. 5.7 had high volume injection (>175 ml acid) and an etched area behind the perforation a factor 500 times bigger than the perforation area. The acid concentration seemed to be of secondary importance, as the patterns created seem governed by the number of acid molecules injected.

6 Impact of Results on Field Scale

The intention in this chapter is to illustrate the impact of some of the data discussed in chapter 4 and 5 on the reservoir scale. The contrast between stress path observations from field and uniaxial strain experiments is addressed in section 6.1. Section 6.2 demonstrates the impact of the laboratory results on reservoir scale by use of a simple subsidence model.

6.1 Stress Path Considerations

The typical North Sea chalk reservoir consists of highly fractured chalk (Andersen, 1995), indicating a reservoir that has already failed in shear when discovered. It is common to assume that producing reservoirs follow a uniaxial strain stress path as the pore pressure is depleted (Fjær et al., 2008). The stress path measured for the cores presented in paper III showed a path following the illustration in Fig. 4.13, i.e. a steep path around 0.3 in the elastic region, which then approach 1.0 during onset of pore collapse and then drop again to a range between 0.4-0.6 in the plastic region. These observations confirm previous results (Leddra et al., 1990; Loe et al., 1992; Jones, 1994). Further, paper III demonstrates that plastic failure in terms of pore collapse and significant deformations are expected when following K_0 conditions.

However, several studies (Teufel and Rhett, 1991; Jupe et al., 2000; Kristiansen et al., 2000; Goulty, 2003; Tjetland et al., 2007) indicate from different perspectives that the reservoir would rather move towards the shear failure surface. Teufel and Rhett (1991), Goulty (2003) and Tjetland et al. (2007) all show field data suggesting a linear stress path in favor of shear failure following a stress path $\Delta\sigma_h/\Delta\sigma_v < 0.2$. Furthermore, observations by micro-seismicity, both from the Ekofisk and Valhall Field suggest that shear failure and re-activation of pre-existing fractures due to production are taking place (Jupe et al., 2000; Kristiansen et al., 2000).

Gutierrez et al. (1992) modeled compaction of a fractured rock mass and showed that plasticity grows from the fractures into the matrix blocks of intact chalk even at low stress path coefficients. Such behavior could be related to the localized deformation seen for SKS 17 in Fig. 4.7. In addition, Teufel and Rhett (1991) suggested that pore collapse could occur in larger weak domains

while the core experienced shear failure on amore global scale. This may suggest that the reservoir stress path and failure mode are somewhat uncertain.

Some of the answer to the difference between laboratory and field observations may be a result of the time dependency of the stress path reviewed in subchapter 4.4. The time dependency suggests that the uniaxial strain path, K_0, decreases with decreasing load rates. In addition, the transition region where K_0 approach 1.0 seems to be shortened, resulting in a more linear path at slower load rates. It could be argued that the reservoir might deform close to the uniaxial strain stress path even if the field stress path is not reproduced in the laboratory tests.

To illustrate this, paper III included a schematic illustration reproduced in Fig. 6.1, where the initial stress state and three possible depleted stress states for the Valhall field have been plotted. The data used in the illustration is based upon published material from the Valhall field (Ruddy et al., 1989; Barkved et al., 2003; Tjetland et al., 2007). The key factor responsible for the variation in the three depleted stress states is a phenomenon called stress arching. The stress arching is giving a contribution of ± 6 MPa to the overburden stress (Kristiansen, 2009). A detailed description of this is given in paper III.

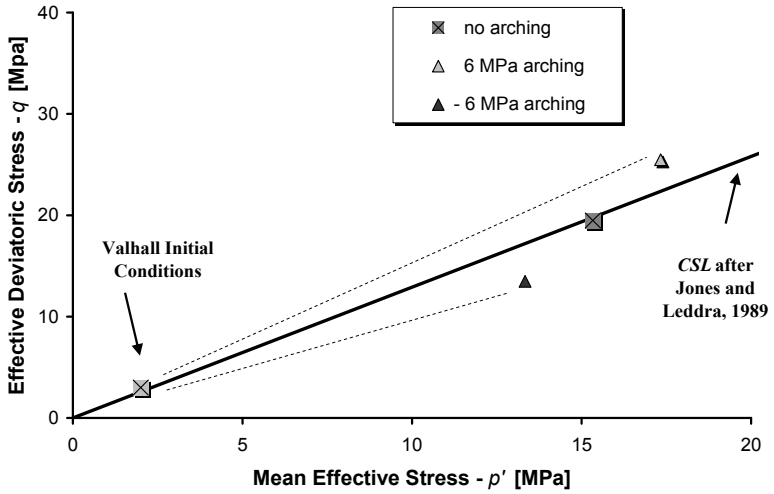

Fig. 6.1. Initial and possible depleted Valhall stress states, compared with an experimentally proposed *CSL*.

The major observation from Fig. 6.1 is that the depleted stress state evolves around the critical state line, *CSL*, for after Jones and Leddra (1989).

Knowing that the stress arching varies throughout the field (Barkved et al., 2003) it is evident that when stress arching contributes to increased vertical stress, the stress state may favor shear failure. With unloading of the overburden the stress state is well below the *CSL*, which is favorable for pore collapse and reservoir compaction. By applying this interpretation of the data, it may be suggested that K_0 for a producing reservoir is simply more linear than traditional experiments suggest due to the experimentally demonstrated time dependency. Due to the stress arching phenomenon, the in-situ K_0 may evolve around the *CSL*.

6.2 Compaction and Subsidence

The laboratory work in this study has focused on quantifying compaction. Compaction of the reservoir rock with resulting subsidence of the surface or seafloor is a natural consequence of oil and gas production, yet for most of these reservoirs the compaction will be negligible (e.g. Fjær et al., 2008). To obtain considerable amounts of subsidence, the factors in Hook's law should be favorable for large changes in reservoir height, h, (i.e. compaction):

$$\frac{\Delta h}{h} = \varepsilon_i = \frac{1}{E}\sigma_i \qquad (6.1)$$

where E is the Young's modulus, ε_i is the directional strain and σ_i is the principal stress in the relevant direction. Both the Ekofisk and Valhall Fields introduced in sub-chapter 1.1 produce from reservoirs with considerable thickness h with soft rock, i.e. low E which corresponds to a high compressibility. Further, these reservoirs experienced a large drop in reservoir pressure, i.e. sufficient change in σ_i. Also the overburden layers need to be taken into account, as they may have different properties than the reservoir, or may be somewhat depleted themselves, or finally may shield the reservoir rock (e.g. Fjær et al., 2008), also called stress arching. Finally, the effect of water weakening should also be mentioned (Risnes, 2001; Madland et al., 2002; Risnes et al., 2003). This subchapter uses a simple subsidence prediction model to visualize the impact of some of the results within this work. The model is called nucleus of strain and was proposed by Geertsma (1973). First, compaction curves for an imaginary reservoir are established.

6.2.1 Reservoir Compaction Curves

The base assumption for the reservoir compaction curves presented within this section is uniaxial strain conditions, K_0. By assuming K_0 conditions, eq. 6.2 may be deduced from eq. 6.1 by using the uniaxial strain modulus H_{el} and H_{pl}, defined in paper III in the elastic and plastic regime respectively.

$$\frac{\Delta h}{h} = \frac{1}{H_{el/pl}} \alpha \Delta p_f \qquad (6.2)$$

where the term $\alpha\Delta p_f$ represents the change in vertical effective stress according to eq. 1.1. By assuming a homogeneous reservoir with a uniform porosity throughout the formation, given that the rock follows linear poroelastic behavior, compaction curves may be plotted using eq. 6.2. Fig. 6.2(a) shows four curves using two different initial porosities; 50% and 35%. The left term in eq. 6.2, has been converted to porosity to make the plot more illustrative. For the two curves with linear modulus in Fig. 6.2(a), the reservoir is believed to follow an elastic trend dictated by H_{el} up to yield, and then a plastic trend dictated by H_{pl} above yield. The values of H_{el}, H_{pl} and uniaxial yield for a 35% and 50% are taken from the published dataset on Maastrichtian chalk by Havmøller and Foged (1996b).

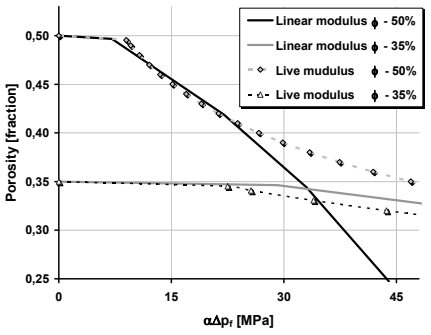

Fig. 6.2(a). Compaction curves for two initial porosities (35% and 50%), using linear modulus (Havmølle and Foged 1996) and live modulus H_{live} (paper III).

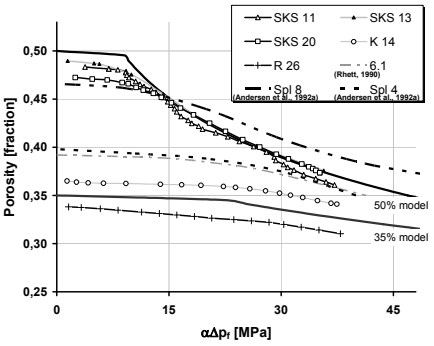

Fig. 6.2(b). Comparing different experimental data (Rhett, 1990; Andersen et al., 1992a; paper III) with the two compaction curves using H_{live}.

Alternatively, the plastic compaction may be predicted using updated moduli values H_{live} according to eq. 4.3. The 50% case represents the upper extreme boundary for the Stevns Klint cores tested and the 35% represents the lower extreme case for the Kansas cores tested. The H_{el} and uniaxial average yield

are based upon the results from Stevns Klint and Kansas in paper III. However, an average yield between yield 1 and yield 2 as defined in Fig. 1.2(b) is used. This was necessary since eq. 6.2 predicts pure plastic behavior once H_{live} is used, and yield 1 only states the onset of the yielding process. For the 50% case a yield point of 9 MPa is defined, whereas for the 35% case 22.5 MPa is defined. H_{el} is set to 1 and 3 GPa for the 50% and 35% curve, respectively, generally based on data from paper III.

The curves predicted by H_{live} are reflecting the non-linear hardening, and the effect of this becomes obvious when looking at the two curves with 50% initial porosity in Fig. 6.2(a). Within this range, *0-45 MPa for* $\alpha\Delta p_f$, the linear modulus predicts the 50% case to approach 25% porosity. As observed from Fig. 6.2(b), experimental data from paper III and other published data (Rhett, 1990; Andersen et al., 1992a), suggest that compaction curves using eq. 6.2 and H_{live} provide a reasonable estimate of reservoir compaction. However, Spl 8 in Fig. 6.2(b) from the study of Andersen et al. (1992a) is not very well predicted. This may be explained by scatter associated with field core testing.

6.2.2 Application of the Subsidence Model

As mentioned in the introduction to this chapter, key observations within this work are studied analytically using the nucleus of strain model proposed by Geertsma (1973). The model is limited to the case where there is no contrast in elastic properties between the reservoir and the surroundings. The reservoir itself is defined as disk shaped in the model. The simplest solution of the model is subsidence in one dimension; the surface displacement w predicted at the centre line of the reservoir, which is given by eq. 6.3 (derived by Fjær et al., 2008);

$$w = 2C_m h \alpha \Delta p_f (1-\nu)\left(1 - \frac{D}{\sqrt{D^2 + R^2}}\right) \qquad (6.3)$$

The reservoir properties in eq. 6.3 are the uniaxial strain compressibility C_m and the effective stress coefficient α. The dimensions of the disk shaped reservoir are given by the thickness h and the radius R. D stands for depth of the reservoir and ν for the Poisson's ratio of the overburden formations.

6.2.2.1 Effect of Porosity Updated Uniaxial Strain Modulus

The thickness of the reservoir is set to 120 m while the radius R is set to 4500 m in radius localized D - 2500 m below the surface. The Poisson's ratio for the overburden is assumed to be 0.3. These parameters are relevant for chalk reservoirs. The reservoir compaction curves in Fig. 6.2(a) represent the reservoir properties in eq. 6.3 and the two porosity cases (50% and 35%) are further shown in the following figures.

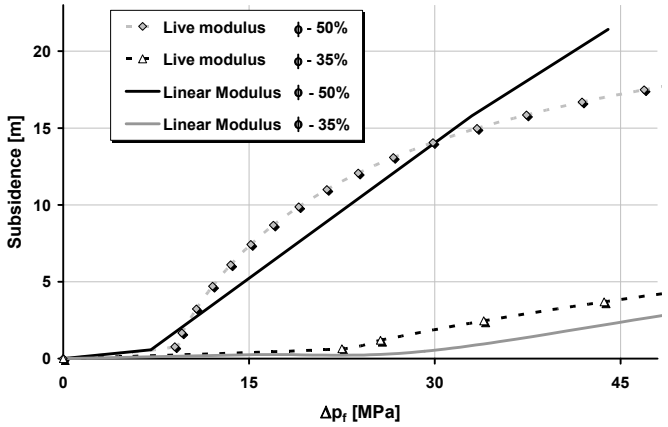

Fig. 6.3. Subsidence along the reservoir centerline using two initial porosities (35% and 50%), using linear modulus (Havmølle and Foged 1996) and live modulus H_{live} (paper III)

Fig. 6.3 plots the subsidence according to eq. 6.3 for the four compaction curves in Fig 6.2(a). The figure illustrates the effect of using linear modulus versus the live modulus H_{live}. First, the elastic response seen from 0 MPa pore pressure depletion to around 9 MPa and to around 22.5 MPa for the 50% and 35% curves respectively produce moderate subsidence response. Then the curves show that a constant plastic modulus, retrieved from the dataset of Havmøller and Foged (1996b), underestimates subsidence compared to the curves predicted using H_{live}, for both the initial 50% and 35% porosity scenarios. However, after around 30 MPa effective vertical stress $\alpha\Delta p_f$ the linear modulus curve for the 50% case exceeds the H_{live} curve.

The Geertsma model emphasizes the significance of the high porosity areas contra the medium porosity areas as contributors to subsidence. While the 35% curves, at 35 MPa depletion, (which equals 35 MPa effective axial stress in the reservoir assuming α - *1*) gives moderate subsidence (1 m for the linear modulus curve and ~2.5 m for the H_{live} curve), the 50% case produces huge subsidence (15.5 m for H_{live} case and around 17 m for the linear modulus case).

6.2.2.2 Influence of the Effective Stress Coefficient

The results from sub-chapter 4.1 (paper I and II) suggest that the effective stress relation is not straight forward for high porosity chalk, especially from a compressibility perspective. To illustrate the effect of a lower effective stress coefficient α on the subsidence, three scenarios with a varying effective stress coefficient, going from 1 to 0.9 and 0.8, are plotted in Fig 6.4(a). The effect for the 50% initial porosity case, at 35 MPa depletion, is around 1 m for each 10% reduction in α. $\alpha = 1$ gives 15.5 m, as in Fig 6.3(b), and $\alpha = 0.9$ and 0.8 result in 14.5 m and 13.5 m subsidence, respectively. For the 35% porosity curves, the equivalent effect was roughly 2.5 m, 2 m and 1.5 m subsidence.

6.2.2.3 Influence of Load Rate

The load rate observations addressed in sub-chapter 4.2 show that load rate effects are detected when tested on relatively high rates 0.02-0.08 MPa/min. However, when going from 31 MPa/day (0.02 MPa/min) to 1 MPa/day, no obvious effects were detected. This last change in rate equals around 29 times reduction. Load rate (or the more frequently used strain rate) data for actual field conditions are neither linear nor uniform throughout the reservoir.

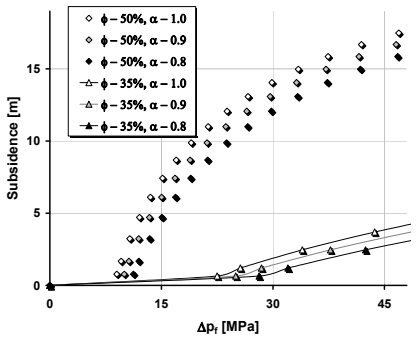

Fig. 6.4(a). Subsidence along the reservoir centerline using two initial porosities (35% and 50%), H_{live} and varying α (1.0, 0.9, 0.8).

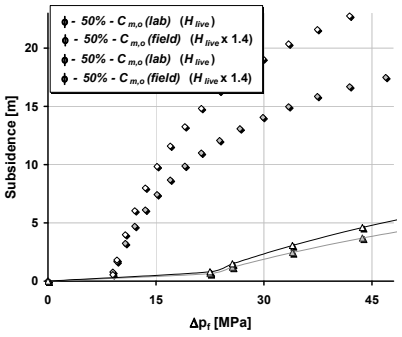

Fig. 6.4(b). Subsidence along the reservoir centerline using two initial porosities (35% and 50%), H_{live} and H_{live} scaled by eq. 6.4.

However, Ruddy et al. (1989) reported that the strain rate at the Valhall field equals 0.0001%/hour, roughly 215 times slower than SKS 20 in Fig. 4.4. Assuming that the entire Valhall field was depleted 31 MPa in 20 years, the load rate would be ~3 x 10^{-6} MPa/min, which is 235 times slower than 0.0007 MPa/min (SKS 20). According to the scaling proposed by de Waal (1986), the

compressibility of the field is related to the compressibility measured in the laboratory according to eq. 6.4:

$$C_{m,o}(field) = \left(\frac{\dot{\sigma}_{z,lab}}{\dot{\sigma}_{z,dep}} \right)^{b} C_{m,o}(lab) \qquad (6.4)$$

$C_{m,o}$ in eq. 6.4 represents the uniaxial compressibility on virgin compaction curves corresponding to different load rates, here field and laboratory rates. The two $\dot{\sigma}_z$ are load rates; the notation $_{dep}$ represents depletion while $_{lab}$ represents laboratory rates. The b-factors are given in section 4.2.1. Using the numbers discussed, $\dot{\sigma}_{z,lab}$ – 0.0007 MPa/min and $\dot{\sigma}_{z,dep}$ – 3x10^{-6} MPa/min, as a factor to scale H_{live} from eq. 4.3, the subsidence influenced by load rate according to de Waal (1989), is plotted in Fig. 6.4(b).

The two curves based upon H_{live} in Fig. 6.3 are used as a base in Fig. 6.4(b). Then, the two curves using scaled compressibility show that additional compaction and subsidence is expected. Pursuing the example of 35 MPa depletion, assuming α = 1, results in roughly 21 m and 3.5 m subsidence for the 50% and 35% case, respectively. This is significantly more than the 15.5 m and 2.5 m predicted using H_{live} in Fig. 6.3.

6.2.2.4 Influence of Uniaxial Creep and Water Weakening

Since time is not a dimension in Geertsma's subsidence model, adjustments are needed to account for uniaxial creep and water weakening. The compressibility C_m, the effective stress coefficient α and the change in pore pressure Δp_f represents reservoir strain in the model, as they are all factors in eq. 6.3. This is seen from eq. 6.2, knowing that C_m is the inverse of $H_{el/pl/live}$. Uniaxial creep may therefore be included by substituting $C_m \alpha \Delta p_f$ by the amount of creep expected. Examples of predicted strain, by the inverse plotting method (Johnson et al., 1989), are given in paper VI or section 5.1.5, which suggests the total expected creep on average to be 5.36%. Paper III suggests that creep is independent of porosity, thus similar amounts of creep are expected for both the 50% and the 35% compaction cases.

It is obvious from the bar illustration in Fig 6.5 that the 5.36% creep has a larger impact on subsidence for the low porosity case. This is a practical consequence of the creep normalization used in paper III. Uniaxial creep is normalized to the reservoir height after depletion, which is significantly different post depletion for the 50% and 35% porosity case. Finally, the effect

of 35 MPa depletion and ultimate creep are 18.6 m and 6.8 m for the 50% and 35% scenario, respectively.

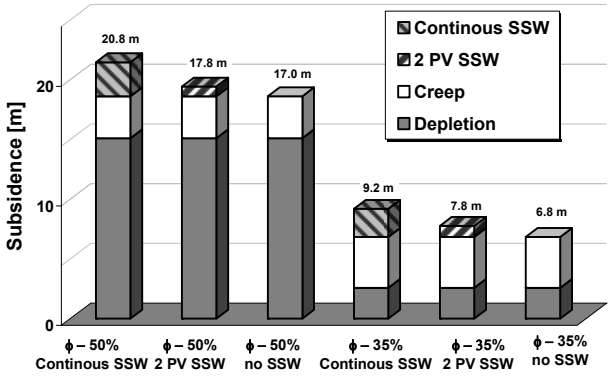

Fig. 6.5. Subsidence along the reservoir center line using two initial porosities (35% and 50%), H_{live} and assuming 5.37% ultimate creep. Comparison of three cases, no SSW, ~3 PV SSW and continuous injection of 3.29 PV SSW/day

Similarly, the effect of water weakening is predicted by the use of the inverse plotting method discussed in section 5.1.5, which predicted 80% additional creep due to continuous injection of 3.29 pore volumes, PV, SSW per day. Such injection scenario would be representative for an extreme case, perhaps only relevant for certain areas near injection wells. This would lead to 20.8 and 9.2 m subsidence, which corresponds to 2.9 m and 2.4 m additional subsidence for the 50% and 35% case, respectively. The most relevant for a water-flooded reservoir would perhaps be injection of around 3 PV of SSW, and section 5.1.5 predicted the corresponding additional creep to 25%. The effect of this on subsidence is rather modest; 0.9 m and 1 m for the 50% and 35% case, respectively.

6.2.2.5 Summary

Fig 6.6 attempts to sum up the various effects of this work on the predicted subsidence by the Geertsma model. Here, the two porosity cases are used, and the curves in the figure are grouping in two clusters, the curves for the 50% case above the curve for the 35% porosity predictions. The upper curve in both clusters is scaled according to eq. 6.4 in section 6.2.2.3. Then below these curves are the basic curves from Fig. 6.3 predicted by using H_{live}. Even less subsidence is expected when α is assumed equal 0.8, which is represented by the black squares and triangles for the 50% and 35% curves, respectively.

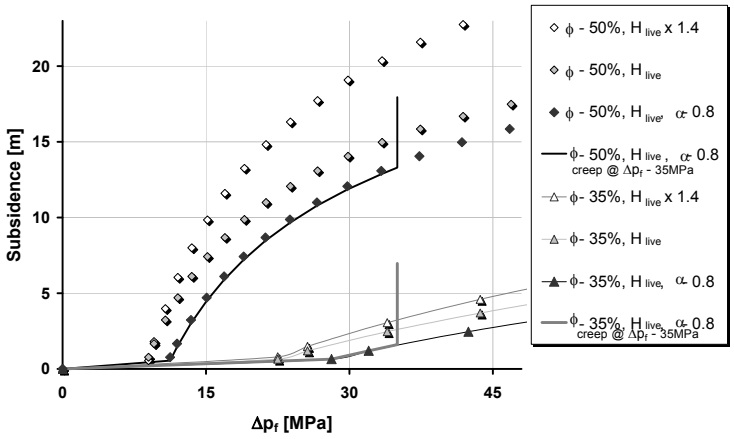

Fig. 6.6. Subsidence along the reservoir center line using two initial porosities (35% and 50%), H_{live} and assuming 5.37% ultimate creep and the effect of ~3 PV SSW.

Finally, the solid lines, the black (50% porosity) and the gray (35% porosity) illustrate a case incorporating the live modulus H_{live}, the effective stress coefficient α equal to 0.8 and creep and water weakening according to injection of around 3 pore volumes of SSW at 35 MPa depletion. The predictions show that the lower porosity case is more sensitive to creep and water weakening. Creep and water weakening caused over 3/4 of the total subsidence. The situation is opposite for the high porosity case, where depletion is responsible for ~3/4 of the total subsidence.

7 Conclusions

This work illustrates the importance of testing at appropriate boundary conditions. This is seen from acid stimulation and the effective stress relationship, where the porosity and strength of the chalk is significant, to fundamental water weakening mechanisms, where the non-carbonate content can be very important. The overall conclusion of this work is that reality may not be described without properly representing the various details.

Effective Stress Relation
Paper I showed that high porosity chalk does not behave according to conventional rock mechanical assumptions regarding effective stress. The experimentally determined effective stress coefficient, α, differs significantly from the theoretically predicted α, using compressibility as the basis for the evaluation. On the other hand, the hydrostatic yield strength of chalk was in paper II shown to follow conventional assumptions, with α close to unity. The apparent conflict between the results from paper I and the results in paper II is explained as effects of the inelastic nature of high porosity chalk which impact the compressibility, yet the yield strength remains unaffected. According to these observations, stress states involving total stresses and pore pressure should be reported as "differential stress" rather than effective stress using an uncertain effective stress coefficient.

Time Dependency during Loading
The experimental results in paper III show that high porosity chalk with similar initial porosity deforms similarly, even though the load rate is dramatically lowered. On the other hand, load rate dependency was proven when the rate of loading was doubled or tripled. This suggests the existence of a lower limit for the load rate effects in high porosity chalk. Paper IV describes compactional failure in chalk as a time dependent reorganization of the grains, and demonstrated that pore collapse is a local mechanism. The experimental results thus confirm the conceptual model called nucleus-of-failure (Andersen, 1995). When this nature of grain reorientation is seen in relation to the load rate effects presented in paper III, it supports the existence of a lower limit for load rate effects. Care should therefore be taken when scaling laboratory load rates to realistic field rates, if a lower limit for load rate effects exists.

Moreover, paper III highlights the importance of initial core porosity, which not only seems to strongly influence the deformation response, but also tends

to describe nonlinear strain hardening by one single relation for the plastic uniaxial strain modulus for chalk from two independent outcrops. The results further indicate that the uniaxial strain stress path is also indirectly dependent on the concept of nucleus-of-failure: Time dependency of the stress path obtained at uniaxial strain conditions was demonstrated, which was linked to the stability of the grain structure during failure. The slower the material is loaded, the more linear and steeper the stress path. The material parameter, the b-factor defined by de Waal (1986) is found equal to 0.04 for Kansas chalk, equivalent to the reservoir chalk tested. In addition, the b-factor was found to be 0.061 for Stevns Klint chalk.

Creep and Water Weakening

The rate at which load was applied seems to be decisive for the transient creep phase, also explained by the nucleus-of-failure concept. Ultimately, this observation is significant, as the absence of transient creep could be interpreted as evidence of no delayed deformation from a former load phase, i.e. a lower limit for load rate effects. Despite the transient creep, paper III shows that the steady state creep seems to be independent of the load rate and porosity. On this basis it is suggested that steady state creep is the true creep that occurs at constant load, separated from the loading phase.

This work confirms the previous studies suggesting that seawater chemically weakens the chalk. This is primarily seen by the effect of injection volume. Paper VI predict 25% additional uniaxial creep when flooding about 3 pore volumes of synthetic seawater, however, an additional 80% uniaxial creep is expected when continuously flooding of about 3 pore volumes per day. Paper V studies the mechanisms behind the chemical water weakening, and shows evidence of newly precipitated minerals. Such precipitation would change the chemical equilibrium in the porous system, which seems to trigger enhanced dissolution of the chalk matrix. Finally, the non-carbonate mineralogy seems to be of significant importance suggesting that appropriate core material is essential when studying chalk water weakening.

Acid Stimulation

The acid stimulation study in paper VII suggests, through visual inspection of acidized cores, that porosity, permeability and material strength influence the etched geometry. The acid seems to spread more easily in higher porosity and softer chalk. Since the chalk-acid reaction is mass transfer limited, this results in dissolution of chalk closer to the entry site of the acid. Similar effects are also seen as the injection flux increases, which seem to spread the acid. The experiments confirm that the acid simply removes the matrix near the inlet.

8 Future Work

A Lower Limit for the Load Rate Effects?
The link between the depletion and transient creep phase demonstrated in chapter 4 is discussed as effects of the time dependent nature of a collapsible failure mode according to the nucleus-of-failure concept. This link suggests that transient creep is a measure of the lag in deformation after a change in load. Transient creep is thus an indicator for load rate effects; as long as transient creep is detected, there is still deformation behavior dependent on the rate of loading.

Proven that such a link exists, a future project is proposed on chalk failure and load rates designed to minimize the transient creep. The creep rate data obtained from such experiments may enter, when presented as in Fig. 4.9(a), directly into the steady state, when and if the effect of transient creep has vanished. The entire deformation would ultimately be driven solely by the increase in load, and not delayed due to the nucleus-of-failure. Ultimately, the true contribution of the loading would then be quantified, also resulting in a higher understanding of the creep processes.

Porosity Influence on Mechanical Behavior
The porosity dependency on deformation behavior demonstrated in section 4.2.2, and on the nonlinear hardening described by eq. 4.3 should be further tested to make the relations more definitive. Similar with the steady state creep in section 4.2.6, that seems to be independent of porosity.

Water Weakening Mechanisms
A comprehensive project on aqueous equilibrium chemistry related to the water weakening phenomenon is currently being supervised by the chalk research group at the University of Stavanger. More work is needed to understand the fundamental mechanisms through the use of SEM-EDS analysis, rock mechanical and core flooding experiments as well as analytical tools such as the Lattice Boltzmann methods. Among other special focus areas that should also be mentioned for future studies are the effect of stepwise repressurizing and water flooding, water induced weakening on fractured chalk and finally, the effect of CO_2 injection on a rock mechanical properties.

9 References

Andersen MA (1995) Petroleum research in North Sea chalk. RF Rogaland Research, Stavanger

Andersen MA, Foged N, Pedersen HF (1992a) The link between waterflood-induced compaction and rate-sensitive behavior in a weak North Sea chalk. Proceedings of 4th North Sea Chalk Sym, Deauville

Andersen MA, Foged N, Pedersen HF (1992b) The rate-type compaction of a weak North Sea chalk. Proceedings of 33rd US Rock Mech Sym, Santa Fe

Alam MM, Christensen HF, Fabricius IL (2009) Effective Stress Coefficient and Biot's Coefficient of Chalk from the Valhall Field, North Sea. Proceedings of SPE EUROPEC/EAGE Ann Conf & Exhib, Amsterdam, SPE 121795-MS

Atkinson JH, Bransby PL (1978) The mechanics of soils: an introduction to critical state soil mechanics. McGraw Hill, London

Barkved O, Heavey P, Kjelstadli R, Kleppan T, Kristiansen TG (2003) Valhall Field – still on plateau after 20 years of production. Offshore Europe, Aberdeen, SPE 83957-MS

Berryman JG (1992) Effective Stress for Transport Properties of Inhomogeneous Porous Rock. J Geophys. Res. 97:17409-17424

Bjerrum L (1967) Engineering geology of Norwegian normally-consolidated marine clays as related to settlements of buildings. Géotechnique 17(2):81–118

Biot MA (1941) General theory of three-dimensional consolidation. J. Appl. Phys. 12(2):155-161

Bishop AW, Henkel DJ (1962) The measurement of soil properties in the triaxial test. Edward Arnold, London

Botter BJ (1985) Pore collapse measurements on chalk cores. Proc 2nd North Sea Chalk Sym, Stavanger

Caldwell CD (1992) Mineralogy and porosity of an Upper Cretaceous chalk sample, Niobrara Formation, W. Kansas. Inter-office correspondence, Phillips Petroleum Company, Bartlesville

Charlez PA (1991) Rock Mechanics: Theoretical Fundamentals, Éditions Technip, Paris

Christensen HF, Foged N, Engstøm F (1992) Absolute horizontal and vertical Permeability Changes under true 3D Reservoir Stress Conditions. Proceedings of 4th North Sea Chalk Sym, Deauville

REFERENCES

Christensen HF (1996) Rock mechanics and water injection – waterflooding of chalk. Proceedings of 5th North Sea Chalk Sym, Reims

Christensen NI Wang HF (1985) The influence of pore pressure and confining pressure on dynamic elastic properties of Berea sandstone. Geophysics 50(2):207-213

De Waal JA (1986) On the rate type compaction behaviour of sandstone reservoir rock. Dissertation, Technische Hogeschool Delft

Dey TN (1986) Permeability and Electrical Conductivity Changes Due to Hydrostatic Stress Cycling of Berea and Muddy J Sandstone. J Geophys Res 91(B1):763-766

Dong C, Hill AD, Zhu D (1999) Acid Etching Patterns in Naturally-Fractured Formations. Proceedings of SPE Ann Tech Conf & Exhib, Houston, SPE 56531-MS

Engstrøm F (1992) Rock mechanical properties of Danish North Sea chalk. Proceedings of 4th North Sea Chalk Sym, Deauville

Fabricius IL (2003) How burial diagenesis of chalk sediments controls sonic velocity and porosity. AAPG Bull. 87(11):1755-1778

Fabricius IL Gommesen L Krogsbøll A Olsen D (2008) Chalk porosity and sonic velocity versus burial depth: Influence of fluid pressure, hydrocarbons, and mineralogy. AAPG Bull. 92(2):201-223

Fatt I (1959) The Biot-Willis elastic coefficients for a sandstone. ASME J Appl Mech. 26:296-297

Fjær E, Holt RM, Horsrud P, Raaen AM, Risnes R (1992) Petroleum related rock mechanics. Elsevier, Amsterdam

Fjær E, Holt RM, Horsrud P, Raaen AM, Risnes R (2008) Petroleum related rock mechanics. Elsevier, Amsterdam

Gauer PR, Sylte JE, Nagel NB (2002) Ekofisk Field Well Log Decompaction. Proceedings of the SPE/ISRM Rock Mech Conf, Irving, SPE 78177-MS

Geertsma J (1973) Land Subsidence Above Compacting Oil and Gas Reservoirs. J Petrol Tech. 25(6):734-744

Gommesen L, Fabricius IL, Mukerji T, Mavko G, Pedersen JM (2007) Elastic behaviour of North Sea chalk: A well-log study. Geophy Prosp. 55:307-322

Goulty NR (2003) Reservoir stress path during depletion of Norwegian chalk oilfields. Petrol Geosci 9:233–241

Gutierrez M, Tunbridge L, Hansteen H, Mukurat A, Barton N, Landa GH (1992) Discontinuum simulation of fractured chalk reservoir behaviour – Ekofisk. Proceedings of 4th North Sea Chalk Sym, Deauville

REFERENCES

Gutierrez M, Øino LE, Høeg K (2000) The Effect of Fluid Content on the Mechanical Behaviour of Fractures in Chalk. Rock Mech Rock Engng 33(2):93-117

Hadizadeh J, Law RD (1991) Water-weakening of Sandstone and Quartzite Deformed at Various Stress and Strain Rates. Int J Rock Mech Min Sci & Geomech Abstr 28(5):431-439

Hatttin DE, Cobban WA (1977) Upper Cretaceous stratigraphy, paleontology, and paleoecology of western Kansas. The Mt. Geol. 14(3-4):175–217

Havmøller O, Foged N (1996a) Advanced rock mechanics stress path testing of chalk. Proceedings of 5th North Sea Chalk Sym, Reims

Havmøller O, Foged N (1996b) Review of rock mechanical data for chalk. Proceedings of 5th North Sea Chalk Sym, Reims

Hellmann R, Renders PJN, Gratier, JP Guiguet R (2002a) Experimental pressure solution compaction of chalk in aqueous solutions Part 1. Deformation behavior and chemistry. Water-Rock Interact, Ore Deposits, and Environm Geochem: A tribute to David A. Crerar (R. Hellmann and S.A. Wood, eds.), Geochem Soc, pp. 129-152

Hellmann R, Gaviglio P, Renders PJN, Gratier JPG, Békri S Adler P (2002b) Experimental pressure solution compaction of chalk in aqueous solutions Part 1. Deformation examined by SEM, porosimetry, synthetic permeability and X-ray computerized tomogratphy. Water-Rock Interact, Ore Deposits, and Environm Geochem: A tribute to David A. Crerar (R. Hellmann and S.A. Wood, eds.), Geochem Soc, pp. 153-178

Hermansen H Thomas LK Sylte JE Aasbøe BT (1997) Twenty Five Years of Ekofisk Reservoir Management. Proceedings of SPE Annual Tech Conf & Exhib, San Antonio, SPE 38927-MS

Heugas O, Charlez P (1990) Mechanical effect of the water injection on Ekofisk chalk. Proceedings of 3rd North Sea Chalk Sym, Copenhagen

Heggheim T, Madland MV, Risnes R, Austad T (2005) A chemical induced enhanced weakening of chalk by seawater. J Petrol Sci Eng 46(3):171-184

Hill AD, Schechter RS (2000) Fundamentals of Acid Stimulation. In: Economides MJ, Nolte KG (eds) Reservoir Stimulation, John Wiley & Sons Ltd, pp 16-(1-28)

Hiorth A, Cathles LM, Kolnes J, Vikane O, Lohne A, Korsnes RI, Madland MV, (2008) A chemical model for the seawater-CO_2-carbonate system – aqueous and surface chemistry. Int Sym SCA, Abu Dhabi

Hjuler ML (2007) Diagenesis of Upper Cretaceous onshore and offshore chalk from the North Sea area. Dissertation, Technical University of Denmark

REFERENCES

Håkansson E, Bromley R, Perch-Nielsen K, (1974) Maastrichtian chalk of north-west Europe – a pelagic shelf sediment. Spec Publs Int Ass Sediment 1:211-233

Janbu N (1985) Soil models in offshore engineering. Géotechnique 35(3):241–281

Jones ME, Leddra MJ, (1989) Compaction and flow of porous rocks at depth. Proceedings Rock at Great Depth, Balkema, Rotterdam 2:891-898

Jones M (1994) Mechanical principles of sediment deformation. In: Maltman A (ed) The geological deformation of sediments, Chapman & Hall, London, pp 37–71

Jones ME (2002) Experimental evaluation and numerical characterization of the pore pressure response of chalks undergoing yield under conditions of restricted fluid drainage. Proj propos subm JCR phase 6, January.

Johnson JP, Rhett DW, Siemers WT (1989) Rock mechanics of the Ekofisk reservoir in the evaluation of subsidence. J Petrol Technol 41(7):717–722

Jupe A, Jones R, Wilson S, Cowles J (2000) The role of microearthquake monitoring in hydrocarbon reservoir management. Proceedings of SPE Annual Tech Conf & Exhib, Dallas, SPE 63131-MS

Korsnes RI, Strand S, Hoff Ø, Pedersen T, Madland MV, Austad T (2006a) Does the chemical interaction between seawater and chalk affect the mechanical properties of chalk? In: Cottheim AV, Charlier R, Thimus JF, Tshibangu JP, (eds) Multiphysics Coupling and Long Term Behaviour in Rock Mechanics. Taylor & Francis, London, pp. 427-434

Korsnes RI, Madland MV, Austad T (2006b) Impact of Brine Composition on the Mechanical Strength of Chalk at high Temperature. In: Cottheim AV, Charlier R, Thimus JF, Tshibangu JP, (eds) Multiphysics Coupling and Long Term Behaviour in Rock Mechanics. Taylor & Francis, London, pp. 133-140

Korsnes RI (2007) Chemical induced water weakening of chalk by fluid-rock interactions – A mechanistic study. Dissertation, University of Stavanger

Korsnes RI, Madland MV, Austad T, Haver S, Røsland G (2008a) The effects of temperature on the water weakening of chalk by seawater. J Petrol Sci Eng 60(3-4):183-193

Korsnes RI, Wersland E, Austad T, Madland MV (2008b) Anisotropy in chalk studied by rock mechanics. J Petrol Sci Eng 62(1-2):28–35

Kristiansen TG, Barkved O, Pattillo PD (2000) Use of Passive Seismic Monitoring in Well and Casing Design in the Compaction and Subsiding Valhall Field, North Sea. Proceedings of SPE Euro Petrol Conf, Paris, SPE 65134-MS

Kristiansen TG, Barkved OI, Buer K, Bakke R (2005) Production-Induced Deformations Outside the Reservoir and Their Impact on 4D Seismic. Proceedings of the International Petroleum Technology Conference, Doha, IPTC 10818-MS

REFERENCES

Kristiansen, TG (2009) Personal communication

Leddra MJ, Jones ME, Goldsmith AS (1990) Laboratory investigation of the compaction of chalk under conditions of increasing effective stress. Proceedings of 3rd North Sea Chalk Sym, Copenhagen

Liingaard M, Augustesen A, Lade PV (2004) Charaterization of Models for Time-Dependent Behavior of Soils. Int J Geomech ASCE 4(3):157-177

Loe N, Leddra M, Jones M (1992) Stress and strain states during chalk deformation. Proceedings of 4th North Sea Chalk Sym, Deauville

Madland MV (1999) Capillary effects in high porosity chalk. Master Thesis, University of Stavanger (HiS)

Madland MV, Korsnes RI, Risnes R (2002) Temperature effects in Brazilian, uniaxial and triaxial compressive tests with high porosity chalk. SPE Annual Tech Conf & Exhib, San Antonio, SPE 77761-MS

Madland MV (2005) Water weakening of chalk - A mechanistic study. Dissertation, University of Stavanger

Madland MV, Finsnes A, Alkafadgi A, Risnes R, Austad T (2006) The influence of CO_2 gas and carbonate water on the mechanical stability of chalk. J Petrol Sci Eng 51(3-4):149-168

Madland MV, Midtgarden K, Manafov R, Korsnes RI, Kristiansen TG, Hiorth A, (2008) The effect of temperature and brine composition on the mechanical strength of Kansas chalk. Proceedings Int Sym SCA, Abu Dhabi

Madland MV, Hiorth A, Korsnes RI, Evje S, Cathles L (2009) Rock Fluid Interaction in Chalk exposed Injection of Seawater, $MgCl_2$, and NaCl Brines with equal Ionic Strength," EAGE, Paris

Malmin, E (1998) Effect of Boundary Conditions on Chalk Compaction. Master Thesis, University of Stavanger (HiS)

Montgomery CT, Ramos GG, Gil I, Ormark K, Soerensen C (2005) Failure Mechanisms in Deepwater Chalks: Rock Stability as Function of Pore Pressure and Water Saturation. Int Petrol Tech Conf, Doha, SPE 10321-MS

Mumallah NA (1991) Factors Influencing the Reaction Rate of Hydrochloric Acid and Carbonate Rock. Proceedings of SPE Int Symp Oilfield Chemi, Anaheim, Paper SPE 21036-MS

Munns JW (1985) The Valhall Field: a geological overview. Mar Petrol Geol 2:23–43

Naugebauer J (1974) Some aspects of cementation in chalk. Spec. Publs int. Ass Sediment 1:149-179

REFERENCES

Newman GH (1983) The Effect of Water Chemistry on the Laboratory Compression and Permeability Characteristics of Some North Sea Chalks. J Petrol Sci Eng 35(5): 976-980

Olsen C (2007) Elastic and electric properties of North Sea Chalk. Dissertation, Technical University of Denmark

Pattillo PD, Kristiansen TG, Sund, GV, Kjellstadli RM (1998) Reservoir compaction and seafloor subsidence at Valhall. Proceedings of SPE/ISRM Eurock Conf, Trondheim, SPE 47274-MS

Pattillo PD, Kristiansen TG (2002) Analysis of Horizontal Casing Integrity in the Valhall Field. SPE/ISRM Rock Mech Conf, Irving, SPE 78204-MS

Pierre A, Lamarche JM, Mercier R, Foissy A, Persello J (1990) Calcium as potential determing ion in aqueous calcite suspensions. J Dispersion Science and Tech 11(6):611-635

Powell BN, Lovell GL (1994) Mechanisms of chalk compaction. Proceedings of SPE/ISRM Rock Mech Petrol Eng Conf, Delft, SPE 28132-MS

Puntervold T, Strand S, Austad T (2007) New method to prepare outcrop chalk cores for wettability and oil recovery studies at low initial water saturation. Energ Fuel 21(6):3425–3430

Rhett DW (1990) Long term effects of water injection on strain in North Sea chalks. Proceedings of 3rd North Sea Chalk Sym, Copenhagen

Risnes R, Gjesdal SA, Landaas TL, Madland I (1994) Changes in mechanical properties of chalk caused by deformation and by pore pressure Proceedings of SPE/ISRM Eurock Conf, Delft, SPE 28136-MS

Risnes R, Kleppa E (1996) Plastic behaviour of high porosity chalk in constant K-ratio tests. Proceedings of 5th North Sea Chalk Sym, Reims

Risnes R, Garpestad OJ, Gilje M, Oland LT, Ovesen M, Vargervik E (1998) Strain hardening and extensional failure in high porosity chalk. Proceedings of SPE/ISRM Eurock Conf, Trondheim, SPE 47581-MS

Risnes R, Flaageng O (1999) Mechanical properties of chalk with emphasis on chalk-fluid interactions and micromechanical aspects. Oil Gas Sci Technol 54(6):751-758

Risnes R, Nygaard V (1999) Elasticity in High Porosity Outcrop Chalk. Sec. Euroconf. Rock Phys. Rock Mech. Heriot-Watt Univers. Edinburgh

Risnes R (2001) Deformation and Yield in High Porosity Outcrop Chalk. Phys Chem Earth (A) 26(1-2):53-57

Risnes R, Haghighi H, Korsnes RI, Natvik O (2003) Chalk–fluid interactions with glycol and brines. Tectonophysics 370(1-4):213-226

REFERENCES

Risnes R, Madland MV, Hole M, Kwabiah NK (2005) Water weakening of chalk – Mechanical effects of water-glycol mixtures. J Petrol Sci Eng 48(1-2):21-36

Robert JA, Crowe, CW (2000) Carbonate Acidizing Design. In: Economides MJ, Nolte KG (eds) Reservoir Stimulation, John Wiley & Sons Ltd, pp 17-(1-15)

Ruddy I, Andersen MA, Pattillo PD, Bishlawl M, Foged N (1989) Rock compressibility, compaction, and subsidence in a high-porosity chalk reservoir: a case study of Valhall Field. J Petrol Technol 41(7):741–746

Scholle PA (1977) Chalk diagenesis and its relation to petroleum exploration: oil from chalks, a modern miracle. AAPG Bull 61(7):982–1009

Schroeder C, Shao J (1996) Plastic deformation and capillary effects in chalks. Proceedings of 5th North Sea Chalk Sym, Reims

Schroeder C, Bois AP, Maury V, Hallé G (1998) Water/chalk (or collapsible soil) interaction: Part II. Results of tests performed in laboratory on Lixhe chalk to calibrate water/chalk models. Proceedings of SPE/ISRM Eurock Conf, Trondheim, SPE 47587-MS

Shafer JL, Boitnott GN, Ewy RT (2008) Effective stress laws for petrophysical rock properties. Proceedings of 49th SPWLA Conference, Edinburgh

Skempton AW (1961) Effective stress in soils, concrete and rocks. In: Pore pressure and suction in soils, British National Society of the International Society of Soil Mechanics and Foundation Engineering. Butterworths, London, pp 4–16

Smith AG Smith TE Monshaugen T (1988) Ekofisk Subsidence: Conceptual and Design Considerations Along the Road to Jacking. Proceedings of 20th Annual Offsh Tech Conf, Houston, OTC-5652-MS

Smith MB, Shlyapobersky JW (2000) Basic of Hydraulic Fracturing. In: Economides MJ, Nolte KG (eds) Reservoir Stimulation, John Wiley & Sons, pp 5-(1-28)

Smits RMM, de Waal JA, van Kooten JFC (1988) Prediction of abrupt reservoir compaction and surface subsidence caused by pore collapse in carbonates. SPE Format Eval 3(2):340–346

Snow SE, Hough EV (1988) Field and Laboratory Experience in Stimulating Ekofisk Area North Sea Chalk Reservoirs. Proceedings of SPE Annual Tech Conf & Exhib, Houston, SPE 18225-MS

Snow SE, Brownlee MH (1989) Practical and Theoretical Aspects of Well Testing in the Ekofisk Area Chalk Fields. Proceedings of SPE Annual Tech Conf & Exhib, San Antonio, SPE 19776-MS

Strand S, Høgnesen EJ, Austad T (2006) Wettability Alternation of Carbonates – Effects of Potential Determining Ions (Ca^{2+} and SO_4^{2-}) and Temperature. Colloids and Surfaces A: Physicochem Eng Aspects, 275:1-10

Sulak RM, Danielsen J (1989) Reservoir Aspects of Ekofisk Subsidenc. J Petrol

Technol 41(7):709-716, SPE 17852-PA

Sylte JE, Thomas LK, Rhett DW, Bruning DD, Nagel NB (1999) Water induced compaction in the Ekofisk Field. Proceedings of SPE Annual Tech Conf & Exhib, Houston, SPE 56426-MS

Terzaghi KV (1923) Die Berechnung der Durchlässugkeitsziffer des Tones aus dem Verlauf der hydrodynamischen Spannungserscheinungen. Sitzungsber. Akad. Wiss. Wien Math. Naturwiss. Kl. Abt. 132(2A):125-138

Teufel LW, Rhett, DW (1991) Geomechanical evidence of shear failure of chalk during production of the Ekofisk Field. Proceedings of SPE 66th Annual Tech Conf & Exhib, Dallas, SPE 22755-MS

Teufel LW, Warpinski NR (1990) Laboratory determination of the effective stress laws for deformation and permeability of chalk. Proceedings of 3rd North Sea Chalk Sym, Copenhagen

Tjetland G, Kristiansen TG, Buer K (2007) Reservoir management aspects of early waterflood response after 25 years of depletion in the Valhall Field. Int Petrol Technol Conf, Dubai, IPTC 11276

Todd T, Simmons G (1972) Effect of Pore Pressure on the Velocity of Compressional Waves in Low-Porosity Rocks. J Geophys Res 77(20)-3731-3743

Van den Bark E, Thomas OD (1981) Ekofisk: first of the giant oil fields in Western Europe. AAPG Bull 65(11):2341–2363

Van den Knaap, W (1959) Nonlinear Behavior of Elastic Porous Media. Petrol. Transact. AIME. 216:179-187, SPE 1124-G

Wiborg R, Jewhurst J (1986) Ekofisk subsidence detailed and solutions assessed. Oil Gas J 84(7):47

York SD, Pong CP, Joslin TH (1992) Reservoir Management of Valhall Field, Norway. J Petrol Tech. 44(8):918-923

Zhang P, Medad TT, Austad T (2007) Wettability alternation and improved oil recovery by spontaneous imbibition of seawater into chalk: Impact of the potential determining ions: Ca^{2+}, Mg^{2+}, and SO_4^{2-}. Colloids Surf A Physicochem Eng Asp 301:199-208

Zangiabadi B, Korsnes RI, Hildebrand-Habel T, Hiorth A, Sutarjana IK, Lian A, Madland MV (2009) Chemical Water Weakening of Various Outcrop Chalks at Elevated Temperature. In: Ling HI, Smyth A, Betti R (eds) Poromechanics IV. DEStech Publications, Lancaster, pp 429–434

Zisman WA (1933) Compressibility and anisotropy of rocks at and near the Earth's surface. Proc Nat Acad Sci 19:666-679

Zoback MD Byerlee JD (1975) Permeability and Effective Stress. AAPG Bull 59(1):154-158